

**Investigation and Optimization of Group III-N
Semiconductor Thin-Film Growths using DC
Nitrogen Plasma**

by

Berek Kadikoff

A Thesis

Presented to Lakehead University

in Partial Fulfillment of the Requirement for the Degree of

Master of Science

in

Electrical and Computer Engineering

Thunder Bay, Ontario, Canada

April 2019

Abstract

The Lakehead University remote plasma-enhanced metalorganic chemical vapour deposition (RPE-MOCVD) reactor utilizes nitrogen plasma to provide the required nitrogen species in group III-N semiconductor material growth. This plasma provides advantages over conventional MOCVD systems, typically using ammonia as the nitrogen source. An issue with using ammonia is that the dissociation temperature is high, restricting the growth of certain materials and limiting possible substrates which may be grown on. The dissociation reaction efficiency of ammonia also plateaus at a low value. With RPE-MOCVD, the system is able to perform growths at significantly lower temperatures, limited only by the metalorganic dissociation temperatures, and the nitrogen plasma species composition and production rates may be varied.

In this work the nitrogen plasma used in the RPE-MOCVD reactor is investigated in order to determine how varying system settings affects plasma conditions. This is done in an effort to optimize group III-N semiconductor thin-film growth conditions in this reactor.

Spectroscopic and Langmuir probe measurements are performed and analyzed as system parameters are varied to investigate the resulting plasma conditions. Experimental GaN growths are performed with varying system parameters on sapphire substrates. The resulting growths are analyzed and compared with the use of X-ray diffraction (XRD), atomic force microscopy (AFM), scanning electron microscopy (SEM), and energy-dispersive X-ray spectroscopy (EDX) characterization techniques.

Acknowledgements

I would like to thank my supervisor, Dr. Dimiter Alexandrov, for the opportunity to be involved in this research and for his continuous support, encouragement, and insight. His openness and support of experimental proposals creates an always stimulating laboratory environment.

I would also like to thank my lab colleagues for their constant support. Their many discussions, explanations, and clarifications were invaluable to understanding the many aspects of the research conducted. Their patience when demonstrating the various laboratory and characterization equipment operational procedures is highly appreciated.

Table of Contents

Abstract.....	i
Acknowledgements.....	ii
Table of Contents.....	iii
List of Figures.....	iv
List of Acronyms.....	vi
1 Introduction.....	1
2 Overview of Thin-Film Growth Methods.....	3
2.1 Metalorganic Chemical Vapour Deposition.....	3
2.2 Overview of Plasma.....	4
2.3 Plasma-Enhanced MOCVD.....	6
2.3.1 Remote Plasma Enhanced MOCVD.....	8
2.4 Lakehead University Remote Plasma-Enhanced MOCVD Reactor.....	8
3 Plasma Characterization.....	12
3.1 Optical Spectroscopy.....	12
3.2 Langmuir Probe Measurements.....	16
4 Experimental Growth Results.....	26
4.1 Growth Considerations and Procedure.....	26
4.2 Characterization Techniques and Results.....	32
4.2.1 X-Ray Diffraction.....	32
4.2.2 Atomic Force Microscopy.....	37
4.2.3 Scanning Electron Microscopy.....	44
4.2.4 Energy-Dispersive X-Ray Spectroscopy.....	55
5 Conclusion and Future Work.....	59
6 References.....	63

List of Figures

Figure 1: CVD Growth Process [4].....	3
Figure 2: Natural and Artificially Produced Plasma[5]	4
Figure 3: Debye Shielding in a Plasma [6]	5
Figure 4: Ammonia Reaction Efficiency [7].....	6
Figure 5: Schematic of Lakehead University Remote Plasma-Enhanced MOCVD Reactor.....	9
Figure 6: Lakehead University Remote Plasma-Enhanced MOCVD System	10
Figure 7: Schematic of Hollow Cathode Plasma Source	10
Figure 8: Migration-Enhanced MOCVD Growth Technique	11
Figure 9: Ignited Nitrogen Plasma	12
Figure 10: Recorded Nitrogen Plasma Spectra at 800W Applied Plasma Power	13
Figure 11: Recorded Atomic Nitrogen Emissions	14
Figure 12: Langmuir Probe Measurement Setup	16
Figure 13: Collected Langmuir Probe Data at 300mTorr, 1000W	18
Figure 14: Langmuir Probe during Ion Collection.....	19
Figure 15: Langmuir Probe during Electron Saturation.....	19
Figure 16: Modified Langmuir Data at 300mTorr, 1000W	21
Figure 17: Calculated Electron Temperatures from Langmuir Probe Measurements	23
Figure 18: Calculated Plasma Densities from Langmuir Probe Measurements.....	24
Figure 19: Average Actual Plasma Power during Growths	28
Figure 20: Atomic Nitrogen Measurements (745nm) at 800W Applied Plasma Power.....	29
Figure 21: Calculated Electron Temperatures at 800W Applied Plasma Power	30
Figure 22: Calculated Plasma Densities at 800W Applied Plasma Power	31
Figure 23: Bragg Diffraction [14].....	32
Figure 24: XRD Results of Best GaN Growths	34
Figure 25: XRD Results of Lower Pressure GaN Growths	35
Figure 26: AFM Operating Principle [16]	37
Figure 27: AFM Result for Growth at 350mTorr, 800W (2 μ m x 2 μ m)	39
Figure 28: AFM Result for Growth at 225mTorr, 800W (2 μ m x 2 μ m)	40
Figure 29: AFM Result for Growth at 450mTorr, 800W (1 μ m x 1 μ m)	41
Figure 30: AFM Result for Growth at 300mTorr, 800W (1 μ m x 1 μ m)	42
Figure 31: Schematic of a Scanning Electron Microscope [17]	45
Figure 32: SEM Operating Principle [18].....	45

Figure 33: SEM Surface-View of GaN Growth at 350mTorr, 800W	46
Figure 34: SEM Surface-View of GaN Growth at 225mTorr, 800W	47
Figure 35: SEM Surface-View of GaN Growth at 350mTorr, 800W with Increased Magnification	48
Figure 36: SEM Surface-View of GaN Growth at 225mTorr, 800W with Increased Magnification	49
Figure 37: SEM Top-View of GaN Growth at 350mTorr, 800W	50
Figure 38: SEM Top-View of GaN Growth at 225mTorr, 800W	51
Figure 39: SEM Cross-Section of GaN Growth at 350mTorr, 800W	52
Figure 40: SEM Cross-Section of GaN Growth at 225mTorr, 800W	53
Figure 41: EDX Operation Principle [19]	55
Figure 42: EDX Result for GaN Growth at 350mTorr, 800W	56
Figure 43: EDX Result for GaN Growth at 225mTorr, 800W	57
Figure 44: Normalized [002] GaN Growth XRD Peaks and Plasma Parameters at 800W Applied Plasma Power	61

List of Acronyms

Metalorganic Chemical Vapour Deposition (MOCVD)

Plasma-Enhanced Metalorganic Chemical Vapour Deposition (PE-MOCVD)

Remote Plasma-Enhanced Metalorganic Chemical Vapour Deposition (RPE-MOCVD)

Light Emitting Diode (LED)

Gallium Arsenide (GaAs)

Gallium Nitride (GaN)

Indium Nitride (InN)

Indium Gallium Nitride (InGaN)

Aluminum Gallium Nitride (AlGaN)

X-ray Diffraction (XRD)

Atomic Force Microscopy (AFM)

Scanning Electron Microscopy (SEM)

Energy-Dispersive X-ray Spectroscopy (EDX)

1 Introduction

The rapid shift into the current information age may be largely attributed to advances in semiconductor material manufacturing. The transistor, a semiconductor device invented at Bell Laboratories in 1947 which resulted in the award of the 1956 Nobel Prize in Physics, is the key component in essentially all modern electronics. With advances in manufacturing processes the performance of these transistors greatly improved along with the achievable device miniaturization, down to the scale of tens of nanometers. The integrated circuit, the development of which revolutionized modern electronics and resulted in the award of the 2000 Nobel Prize in Physics, consists of millions or even billions of transistors on a single chip. The realization and continued improvement of these devices circuits are the result of the advancement of many processes involved in the semiconductor device fabrication methods.

The silicon typically used in the production of these integrated circuits is unsuitable for some applications however. Silicon has an indirect bandgap, resulting in the radiation of energy away in the form of vibrational energy, which makes it unsuitable for use in optical devices. Semiconductor materials with the required direct bandgaps, where energy is radiated away in the form of photons, for use in optical devices includes the group III-V compounds such as GaAs. More recently the group III -N materials, such as GaN, have been the subject of research for use in various devices.

Advances in group III-N semiconductor material processing have allowed for the fabrication and improvement of many electronic devices which have an appreciable impact on our everyday lives. A notable example is the GaN blue light emitting diode (LED), the development of which resulted in the award of the 2014 Nobel Prize in Physics, and the

subsequent development of the InGaN white LEDs which allows for an enormous reduction in the power consumption for residential and commercial lighting purposes among other uses [1]. The emergence of quantum well semiconductor lasers utilizing materials such as AlGaIn have led to improvements in high-efficiency semiconductor lasers with low threshold currents which may be found optical communication systems, applications of which include long-distance internet connections [2]. The development of AlGaIn/GaN high mobility electron transistors provides a high-frequency, high-gain, and high-speed transistor useful for microwave systems such as those used for satellite communications [3].

The advancement and optimization of the epitaxial growth methods of these materials is a key factor in the realization of these III-N devices. The utilization of nitrogen plasma for the growth of the III-N materials provides unique advantages over systems using only thermal processes. However, with the introduction of plasma to the system, additional growth process and system parameter considerations must be made.

As the conditions of the generated plasma used will affect the resulting growths, the relationship between varying system parameters, plasma conditions, and resulting III-N semiconductor thin-film growth quality are investigated in this work.

2 Overview of Thin-Film Growth Methods

2.1 Metalorganic Chemical Vapour Deposition

Metalorganic chemical vapour deposition (MOCVD) is a thin-film epitaxial growth technique performed in heated growth chambers under vacuum utilizing metalorganic chemical precursors and other gas-phase reactants. The main processes in MOCVD growth can be seen in Figure 1.

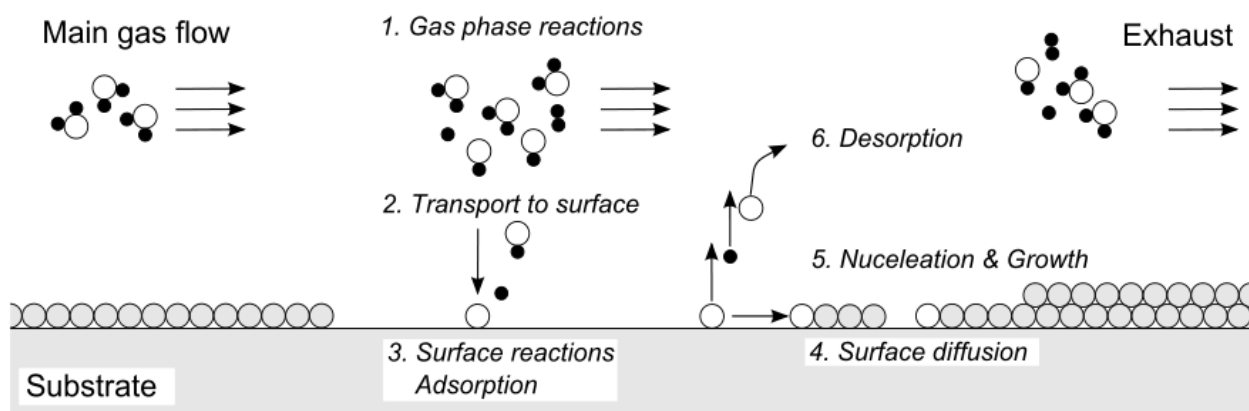


Figure 1: CVD Growth Process [4]

As shown in Figure 1, as the metalorganic precursor is introduced into the heated growth system it disassociates above a certain temperature. The resulting metal species is then deposited onto a substrate and surface reactions such as adsorption and diffusion along the substrate occur. If conditions suitable for growth are achieved in the chamber, growth site nucleation may begin and subsequent crystal growth may be achieved. At the end of the growth cycle, the remaining organic ligands from the precursor molecules and any adatoms which may have desorbed are exhausted from the system.

To produce GaN from an existing Ga layer on a substrate, a nitrogen source, typically ammonia, would be introduced and disassociated by the heated chamber. The nitrogen species is then incorporated into the existing deposited metal layer and a GaN layer is formed. This process may then be repeated to achieve a desired overall growth layer thickness. There are limitations to this thermal-based process which may be overcome with the utilization of plasma which will be discussed in the following sections.

2.2 Overview of Plasma

Plasma, which is sometimes referred to as the fourth, most universally abundant, state of matter, is essentially a gas which has been sufficiently heated to become ionized. What is meant by ionization here is that the hot gas has been disassociated, resulting in a system consisting of both ionized gas species and free electrons. Shown in Figure 2, the densities and electron temperatures, in units of electron-volts where $1\text{eV} \approx 11,600^\circ\text{K}$, for various naturally occurring and artificially produced plasmas are shown.

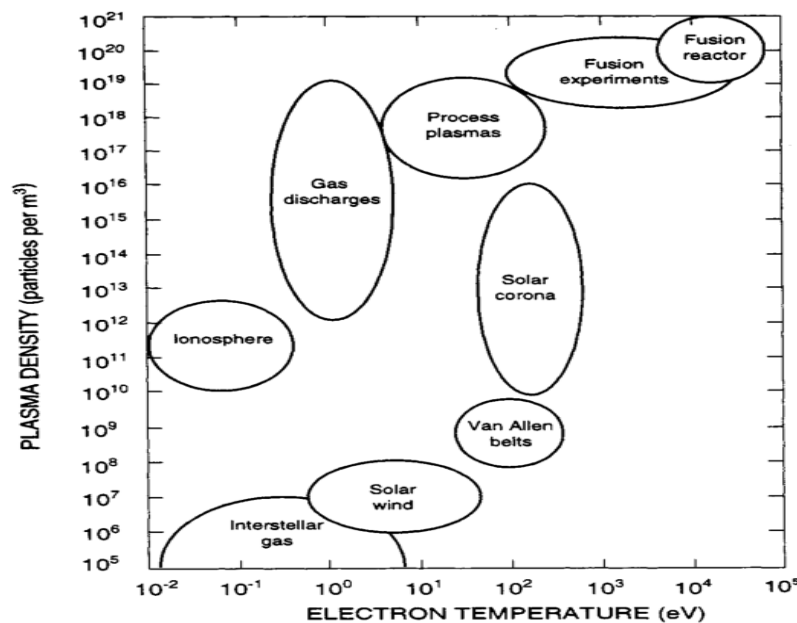


Figure 2: Natural and Artificially Produced Plasma[5]

As can be seen in Figure 2, plasma conditions may vary with a wide range of particle densities and temperatures. Plasma can be found with low densities and relatively low temperatures when observed in interstellar space or in fluorescent tubes. Plasmas may also be found with extremely high temperatures which drive the thermonuclear reactions occurring in the cores of stars such as our sun, and as required in nuclear fusion reactors.

Plasma can more formally be described as a “quasineutral gas of charged and neutral particles which exhibit collective behaviour” [6] existing typically in a vacuum. If not in a vacuum the plasma may be cooled by air, resulting in the ion and electrons recombining into neutral atoms.

What is meant by quasineutrality is that the overall ion and electron densities of the plasma are equal. Overall, $n_p \approx n_i \approx n_e$ where n_p is the overall plasma density, n_i , is the ion density, and n_e is the electron density. This quasineutrality is maintained by a process known as Debye shielding.

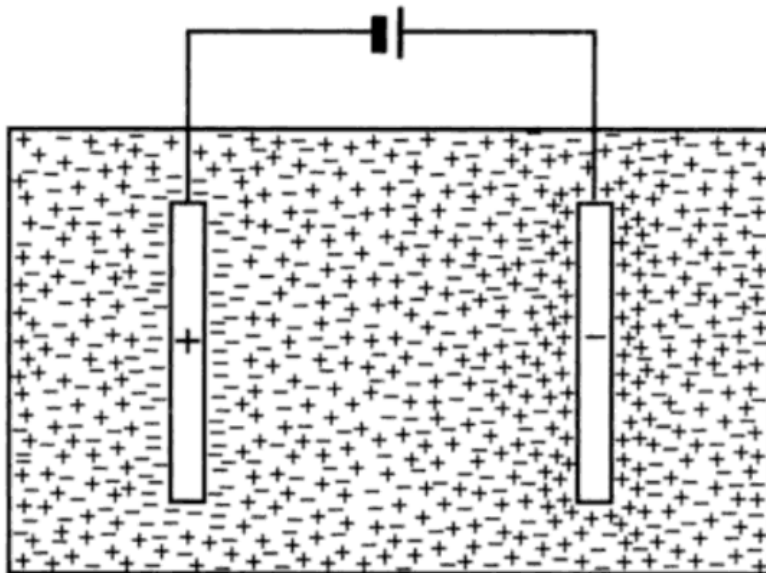


Figure 3: Debye Shielding in a Plasma [6]

The process of Debye shielding, shown in Figure 3, prevents any accumulations of incoming charges. This is achieved as sheaths of electrons or ions are formed at the terminals of an externally applied potential, forcing the incoming charges out and maintaining overall plasma neutrality.

The collective behaviour observed in plasma arises from the dominating interactions between the many charged particles in the plasma. The long-range electrostatic force, known as the Coulomb force, between the ions and electrons dictates plasma behaviour

2.3 Plasma-Enhanced MOCVD

The utilization of nitrogen plasma to provide the nitrogen species for III-N growth rather than the nitrogen-containing compound ammonia, which is commonly used in MOCVD processes, has several advantages. A major advantage is the elimination of the lower growth temperature limit set by the inefficient dissociation of ammonia. To crack ammonia a minimum temperature of 500°C is required and the reaction efficiency plateaus at 3.8% at 700°C, seen in Figure 4 [7].

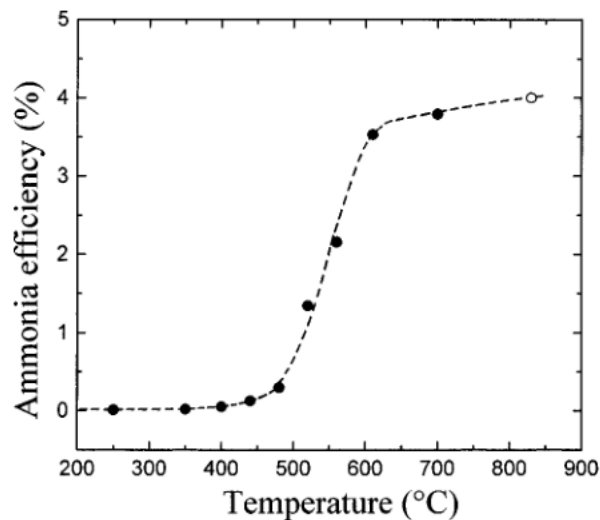


Figure 4: Ammonia Reaction Efficiency [7]

While using nitrogen plasma, the lower temperature limit depends only on the metalorganic dissociation temperature and higher nitrogen species production efficiency is expected. The ability to grow III-N layers at lower temperatures presents the opportunity to use substrates which would otherwise be damaged by the required higher temperatures, such as glass, existing growth structures, or metallic surfaces. The reduced temperature requirement also makes a plasma-based system more suitable for indium nitride growth as the decomposition of InN begins to occur at 500°C, near the initial dissociation temperature of ammonia [8].

Another advantage of plasma-enhanced MOCVD over conventional MOCVD is the improved density of the resulting deposited thin-films. As plasma species bombard the growth sample, atoms on the exposed surface may be forced down to fill voids in the underlying layers [9].

However, if the kinetic energy of the plasma species, the plasma temperature, is sufficiently high the deposited material could be ejected from the surface upon plasma bombardment in a process known as sputtering. Plasma sputtering can be used for material deposition as well by bombarding a target material source, such as an aluminum disk, and having the ejected material be deposited onto a surface. This process is also used in integrated circuit production for selective etching of device layers and for reducing the surface roughness of materials.

In addition to the possible plasma damage to growth surfaces, the utilization of plasma-assisted growth methods introduces other variables which must be considered when performing epitaxial growths. The plasma composition, temperature, density are all variable and dependent

on the selected system parameters such as the chamber pressure and the required applied voltage to ignite the plasma.

The potential plasma etching of growth surfaces is a major concern when using plasma-enhanced MOCVD methods as the deposited material may be getting ejected from the growth surface. In attempts to avoid this etching, a growth method known as remote plasma-enhanced MOCVD is used.

2.3.1 Remote Plasma Enhanced MOCVD

In remote plasma-enhanced MOCVD growth methods the plasma is produced externally from the growth chamber. The plasma source is sufficiently far away from where the growth substrates in attempts to allow highly energetic species in the plasma to decay and prevent damaging, and potentially etching, the growth surface.

2.4 Lakehead University Remote Plasma-Enhanced MOCVD Reactor

A schematic of the unique Lakehead University remote plasma-enhanced MOCVD reactor is shown in Figure 5 and the main components can be seen in Figure 6. The growth chamber is held under vacuum by turbomolecular and rotary pumps. The load lock allows the growth chamber to remain under vacuum while samples are loaded and unloaded. The precursor cabinet houses the metalorganic precursors and dopant sources. The control cabinet controls all system parameters of the system such as chamber pressure, gas pulse timings, number of growth cycles and temperature during growths.

In the hollow cathode plasma source, shown in Figure 7, a sufficient DC voltage is applied to a flow of pure nitrogen gas to generate nitrogen plasma consisting of atomic, ionic and other active nitrogen species.

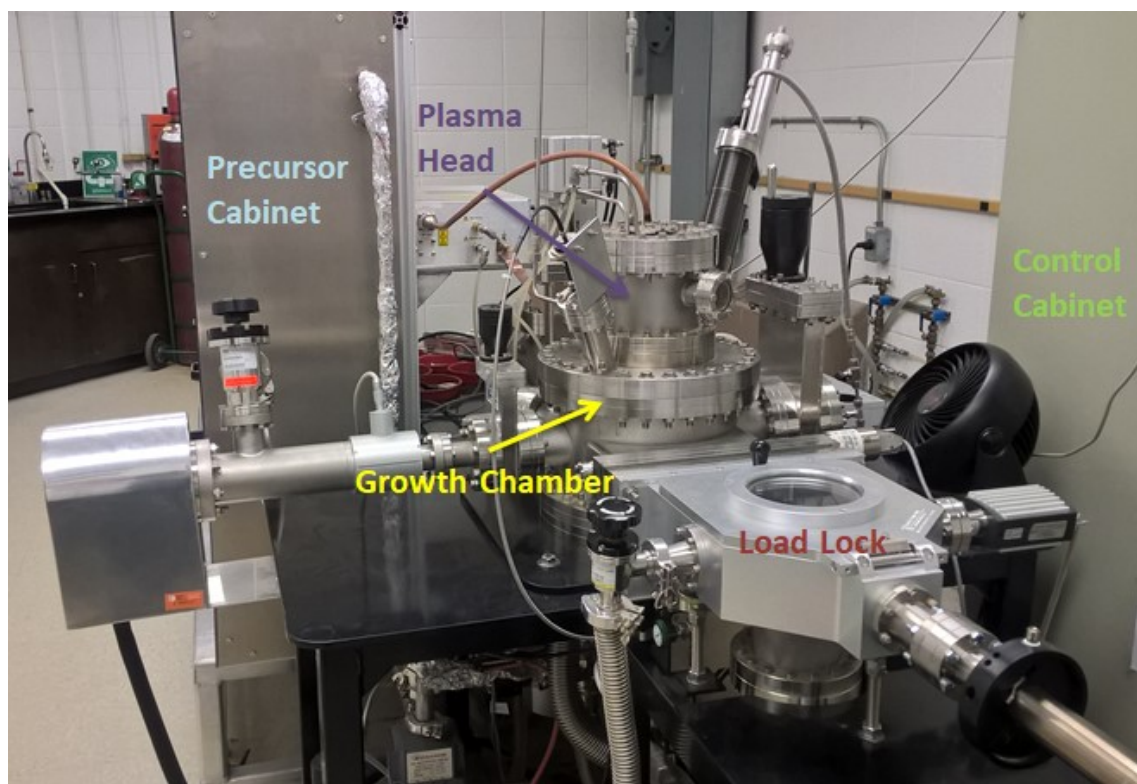


Figure 6: Lakehead University Remote Plasma-Enhanced MOCVD System

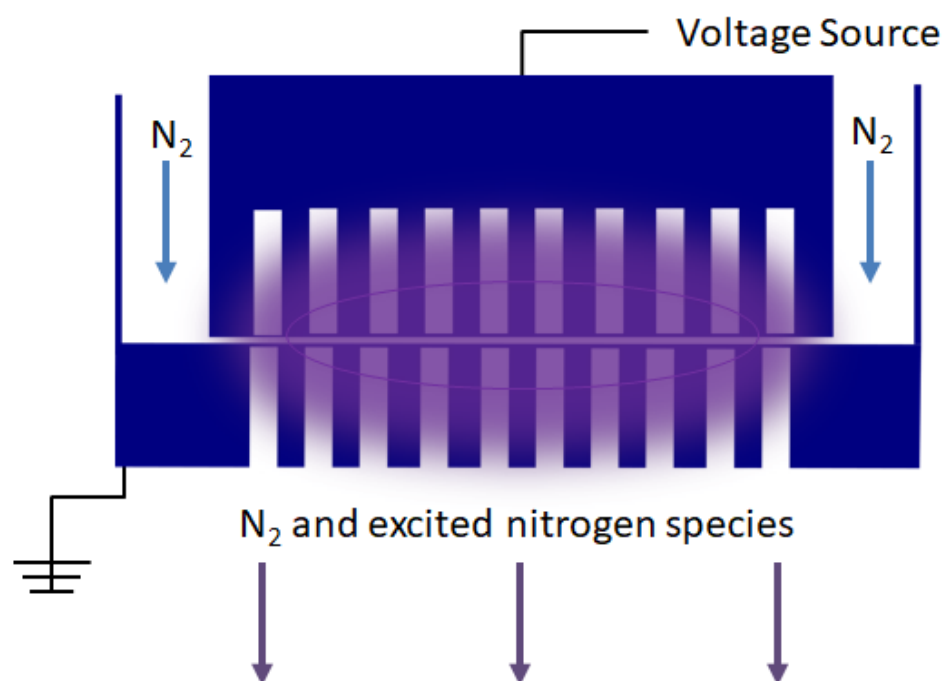


Figure 7: Schematic of Hollow Cathode Plasma Source

In addition to utilizing a remote plasma source for the nitrogen species, the Lakehead reactor uses a migration-enhanced technique growth technique. As opposed to introducing both the metalorganic and nitrogen source simultaneously as with conventional MOCVD, the migration-enhanced method, shown in Figure 8, alternatively pulses the precursor and nitrogen source. By pulsing the metalorganic precursor and the nitrogen, time is allowed for the migration of the metallic adatoms along the substrate surface, enhancing two-dimensional growth [10].

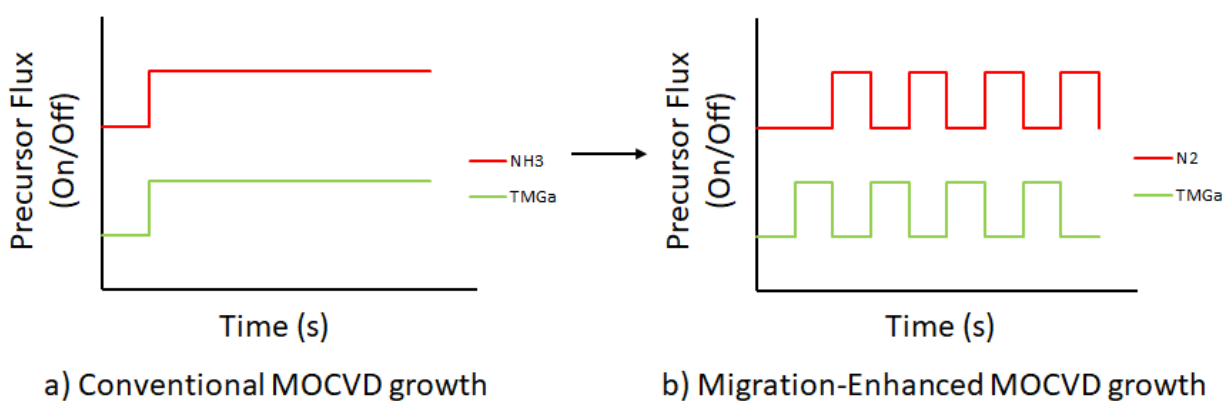


Figure 8: Migration-Enhanced MOCVD Growth Technique

3 Plasma Characterization

3.1 Optical Spectroscopy

In order to study the composition of the nitrogen plasma, spectroscopic data was recorded at various chamber pressures and applied plasma powers with a spectrometer. The composition of the plasma can be determined by comparing the wavelengths of the resulting spectral peaks with the known wavelengths of emissions from specific electronic transitions.

The ignited nitrogen plasma in the Lakehead reactor is seen in Figure 9. The resulting spectra where the three highest atomic nitrogen emission measurements were found are shown Figure 10 and an expanded view of the atomic nitrogen emissions region is seen in Figure 11.



Figure 9: Ignited Nitrogen Plasma

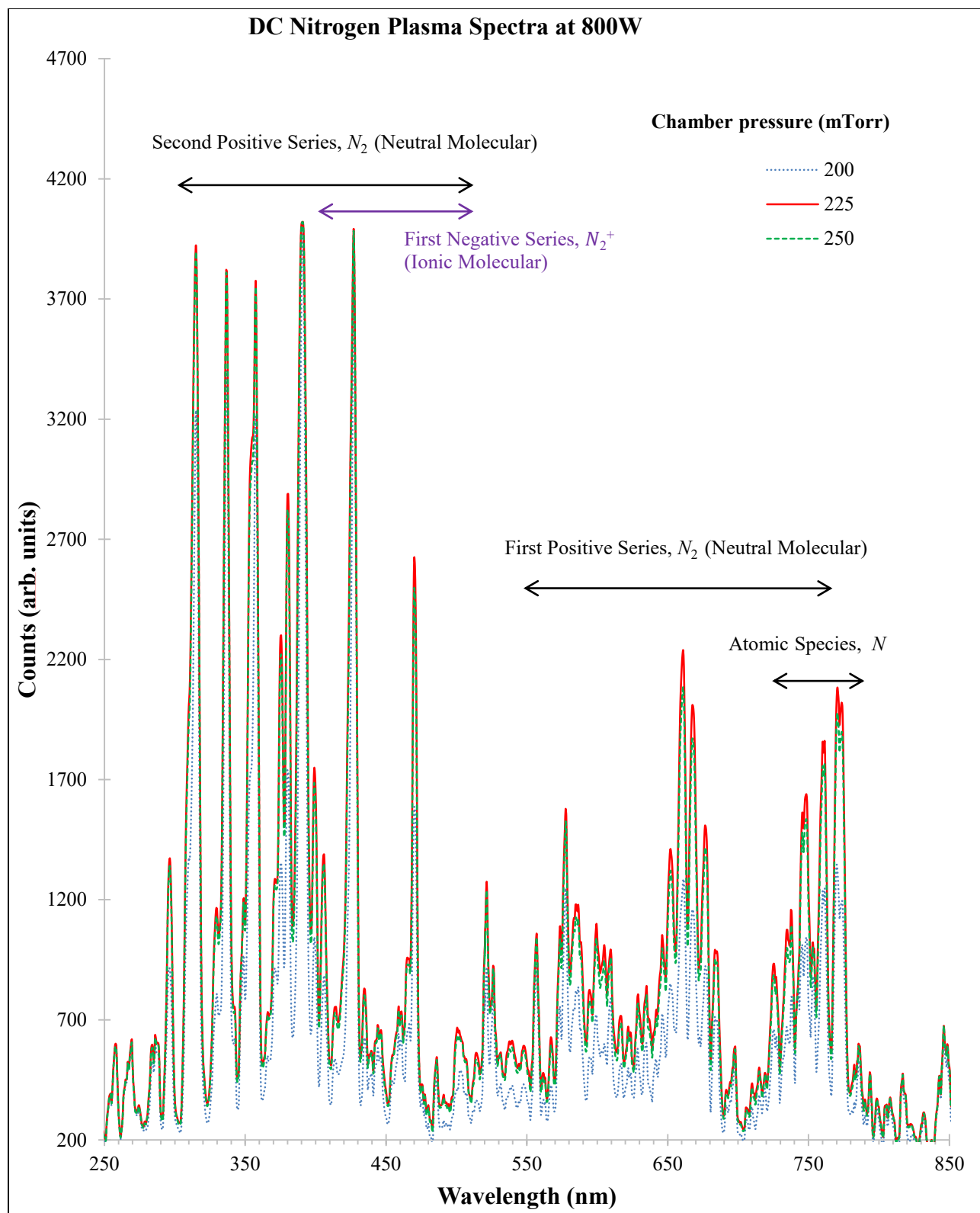


Figure 10: Recorded Nitrogen Plasma Spectra at 800W Applied Plasma Power

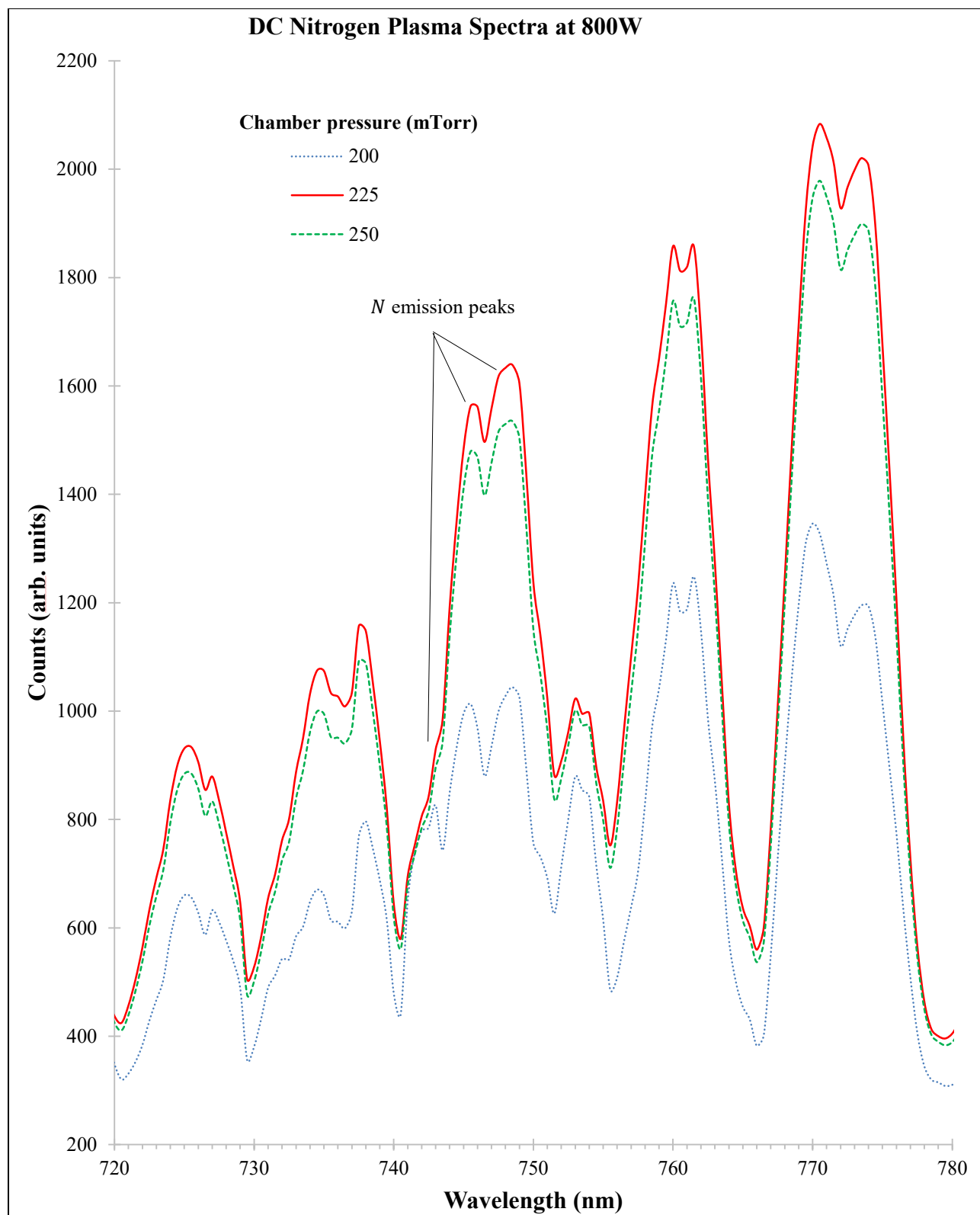


Figure 11: Recorded Atomic Nitrogen Emissions

Shown in Figure 10, the plasma composition was found to be dominated by peaks corresponding to ionic molecular nitrogen, resulting in the violet emissions seen in Figure 9, and neutral molecular nitrogen species [11]. The second and first positive series for neutral molecular nitrogen species emissions are seen from roughly 300 – 500nm and 540 – 755nm respectively. The first negative series for ionic nitrogen species emissions are seen from roughly 380 – 500nm. It has been investigated elsewhere and reported that the neutral molecular nitrogen species does not appear to contribute to III-N crystal growth [12].

The peaks seen in Figure 11 correspond to the $3s^4P \rightarrow 3p^4S^0$ atomic nitrogen transitions at 742.3nm, 744.2nm, and 746.8nm along with sidebands resulting from molecular rotational and vibration states [11].

It was found that as chamber pressures were increased beyond 250mTorr the measured atomic nitrogen emission counts continued to decrease beyond the measured values seen for 200mTorr. At an applied plasma power of 800W the highest atomic nitrogen emissions were measured at chamber pressures of 225, 250, and then 200mTorr.

As the peak atomic nitrogen content was observed at 225mTorr, 800W applied plasma power, it is hypothesised that using these chamber parameters will result in favourable conditions for III-N crystal growth.

3.2 Langmuir Probe Measurements

To investigate the plasma temperature and density at various chamber pressures and applied plasma powers, Langmuir probe measurements were performed and analyzed using an experimental setup depicted in Figure 12.

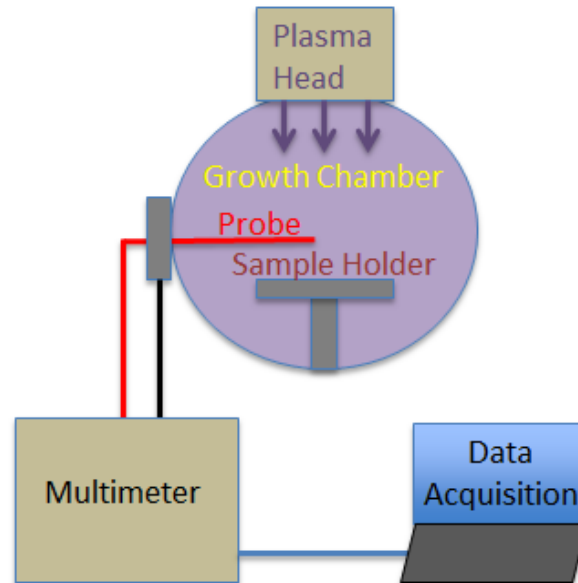


Figure 12: Langmuir Probe Measurement Setup

A Langmuir probe is a thin metallic rod capable of withstanding the high particle temperatures in plasma with all but a small tip at the end of the probe encased in an isolating material. The probe used for these measurements is a cylindrical tungsten rod encased in a ceramic insulator and was immersed in the plasma 9cm from the plasma source.

When immersed in the plasma and an external voltage is applied, the probe tip collects ions or electrons depending on the polarity of the applied voltage. The resulting probe current is recorded and the electron temperature and plasma density can be determined using analytical methods which will be further discussed.

Chamber pressures were varied from 100 – 600mTorr in 100mTorr steps and the applied plasma power was varied from 600 – 1000W in 100W steps. A multimeter supplied the probe voltages which gradually increased from -50V to 50V and the collected probe currents were measured. The raw collected data at a chamber pressure of 300mTorr and an applied plasma power of 1000W is seen in Figure 13.

As a negative voltage is applied to the probe, positive ions are collected and a small negative current is collected, seen in the collected data in Figure 13. Figure 14 shows the probe during these low current measurements producing no noticeable effect. As a positive voltage is applied electrons are collected, resulting in a rapid rise in current as the voltage increases until electron saturation occurs, seen in sharp rise in the collected data in Figure 13. Figure 15 shows the probe as the collected current quickly rises which can be visibly observed as probe tip begins to glow.

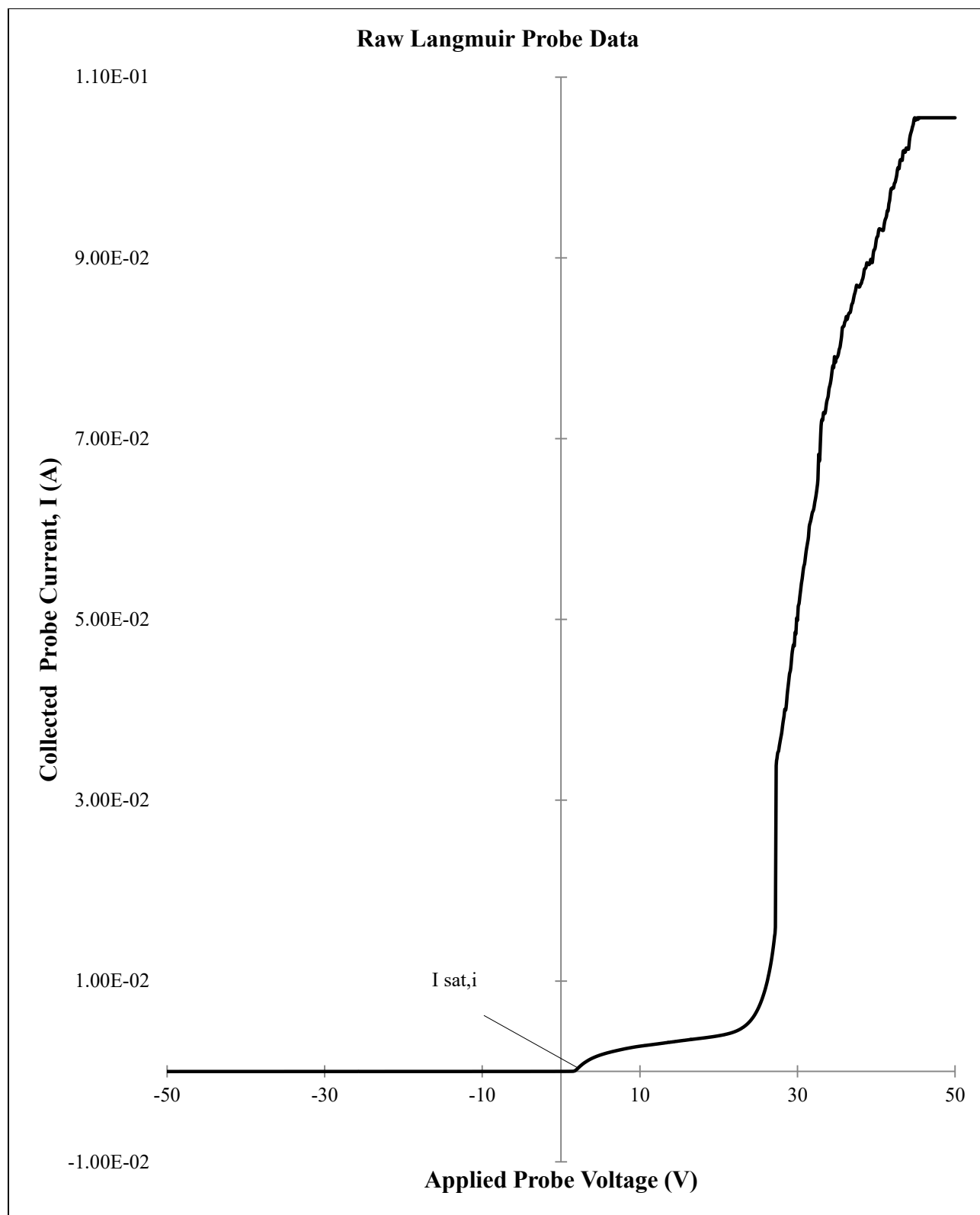


Figure 13: Collected Langmuir Probe Data at 300mTorr, 1000W

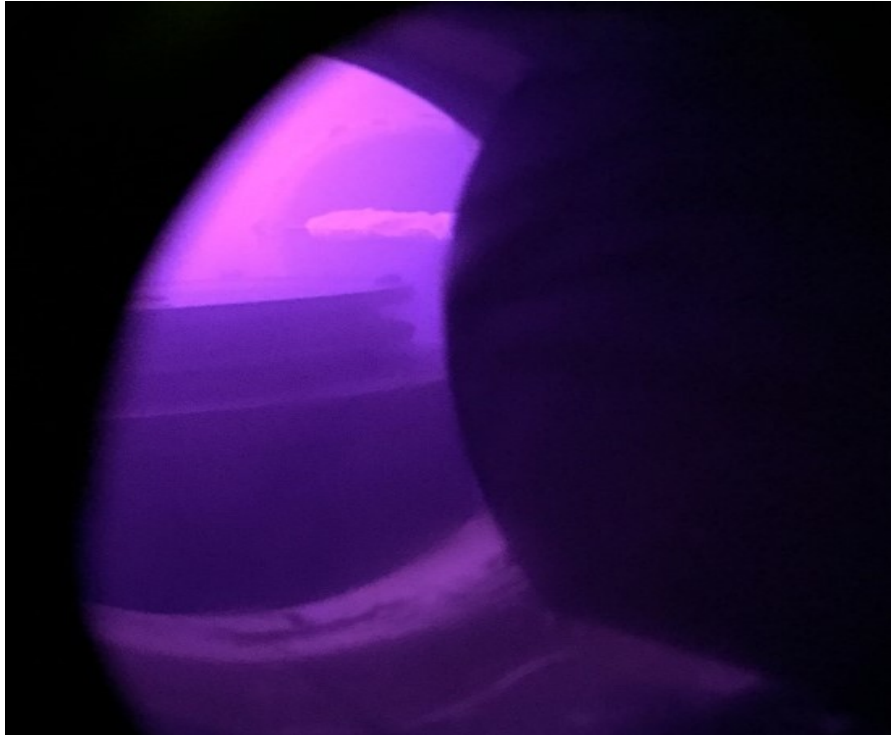


Figure 14: Langmuir Probe during Ion Collection

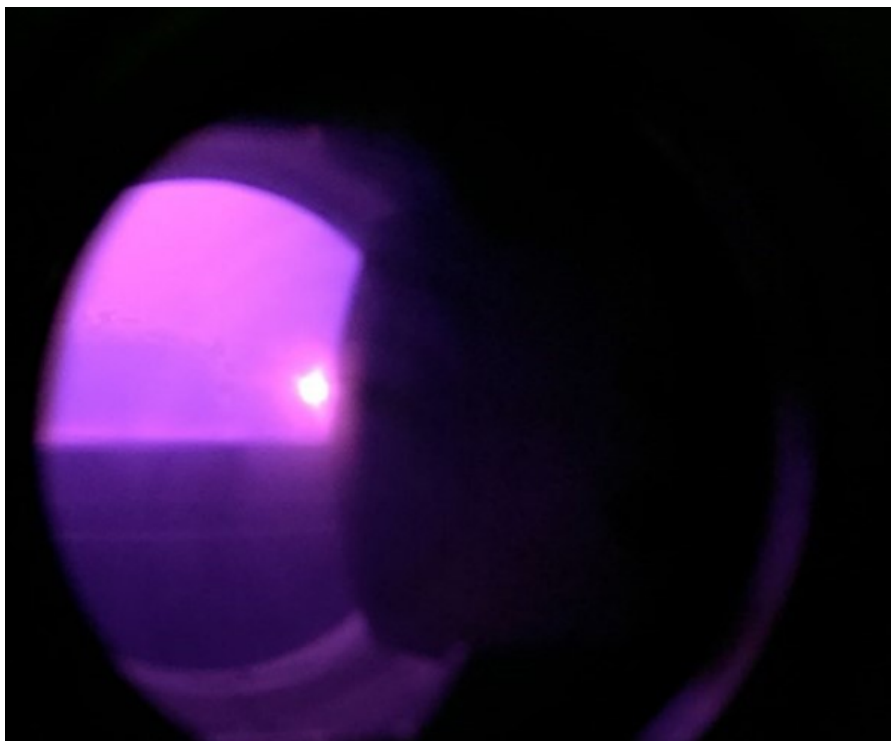


Figure 15: Langmuir Probe during Electron Saturation

Following methods presented in [13], the electron temperature, T_e , is found by starting with the following expression.

$$\frac{1}{T_{e(eV)}(V-V_f)} = \ln |I - I_{sat,i}| \quad (1)$$

Here $T_{e(eV)}$ is the electron temperature in electron volts given by $T_{e(eV)} = \frac{k}{q} T_{e(^{\circ}K)}$ with $T_{e(^{\circ}K)}$ being the electron temperature in degrees Kelvin, k is Boltzmann's constant, q is electron charge, V is the applied probe voltage, and V_f is floating potential which is the applied voltage resulting in zero total current. The floating potential is nearly zero for all performed experiments in this work.

The ion saturation current, $I_{sat,i}$, is determined by locating the point where the collected probe current rapidly rises from negative to positive, shown in Figure 13. Then, the raw data is modified by plotting the applied probe voltage versus $\ln |I - I_{sat,i}|$, shown in Figure 16.

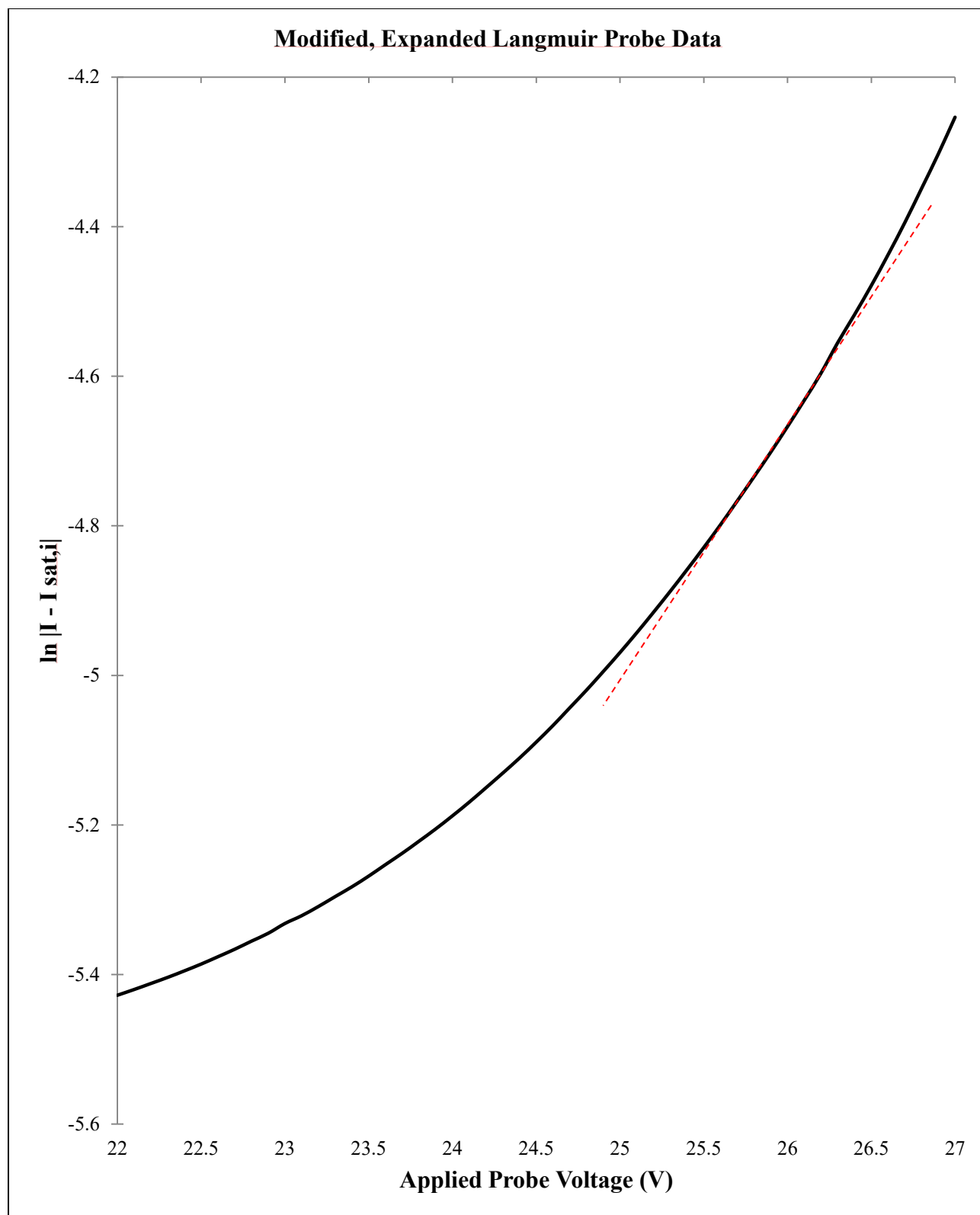


Figure 16: Modified Langmuir Data at 300mTorr, 1000W

The maximum rate of change of the electron saturation transition region, shown by the dashed line in Figure 16, is then determined and used to calculate the plasma temperature. This calculation can be expressed by the following equation.

$$T_{e(eV)} = \left(\frac{d}{dV} (\ln|I - I_{sat,i}|)_{Max} \right)^{-1} \quad (2)$$

With the electron temperature known, the plasma density, n_p , can be then calculated using the following expression [6].

$$n_p = \frac{|I_{sat,i}|}{qA_s e^{-\frac{1}{2}} \sqrt{T_{e(eV)}}} \sqrt{\frac{qM}{e}} \quad (3)$$

Here $A_s \approx 2.162 \mu m^2$ is the exposed probe tip surface area, e is the exponential function, and M is the mass of nitrogen, determined to be $M = \frac{14(\frac{g}{mol})}{N_A} = 2.32 \cdot 10^{-26} kg$, with N_A being Avogadro's number.

The ion saturation current and the maximum rate of change of the electron saturation current region were found using Matlab. The resulting electron temperatures and densities for Langmuir probe measurements are shown in Figure 17 and Figure 18. The anomalous data point seen at a chamber pressure of 400mTorr, 800W applied plasma power will be treated as an outlier from any observed general trends for electron temperature behaviour. This sharp rise and fall of electron temperature is not found at any other pressure-power settings from the overall collected data.

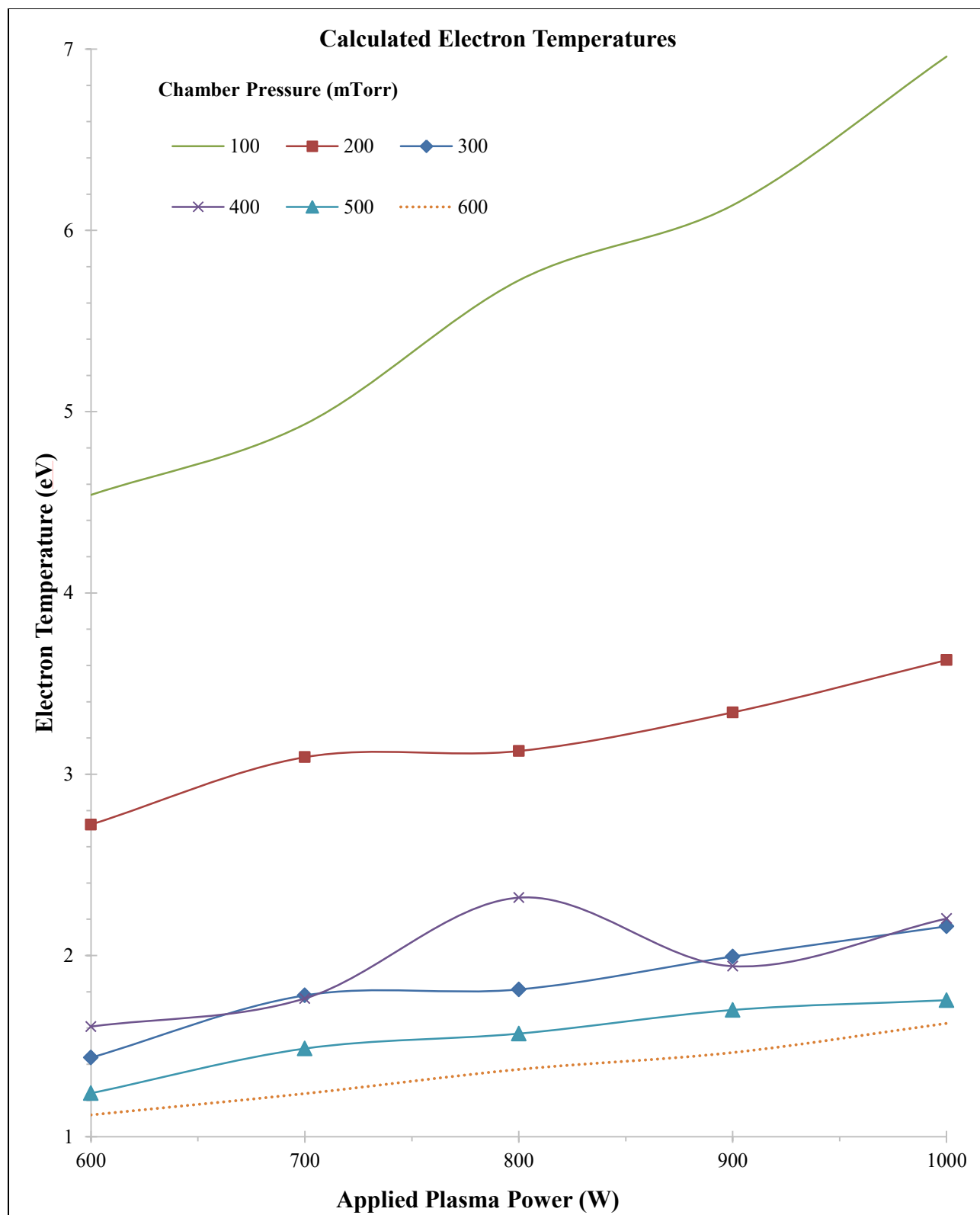


Figure 17: Calculated Electron Temperatures from Langmuir Probe Measurements

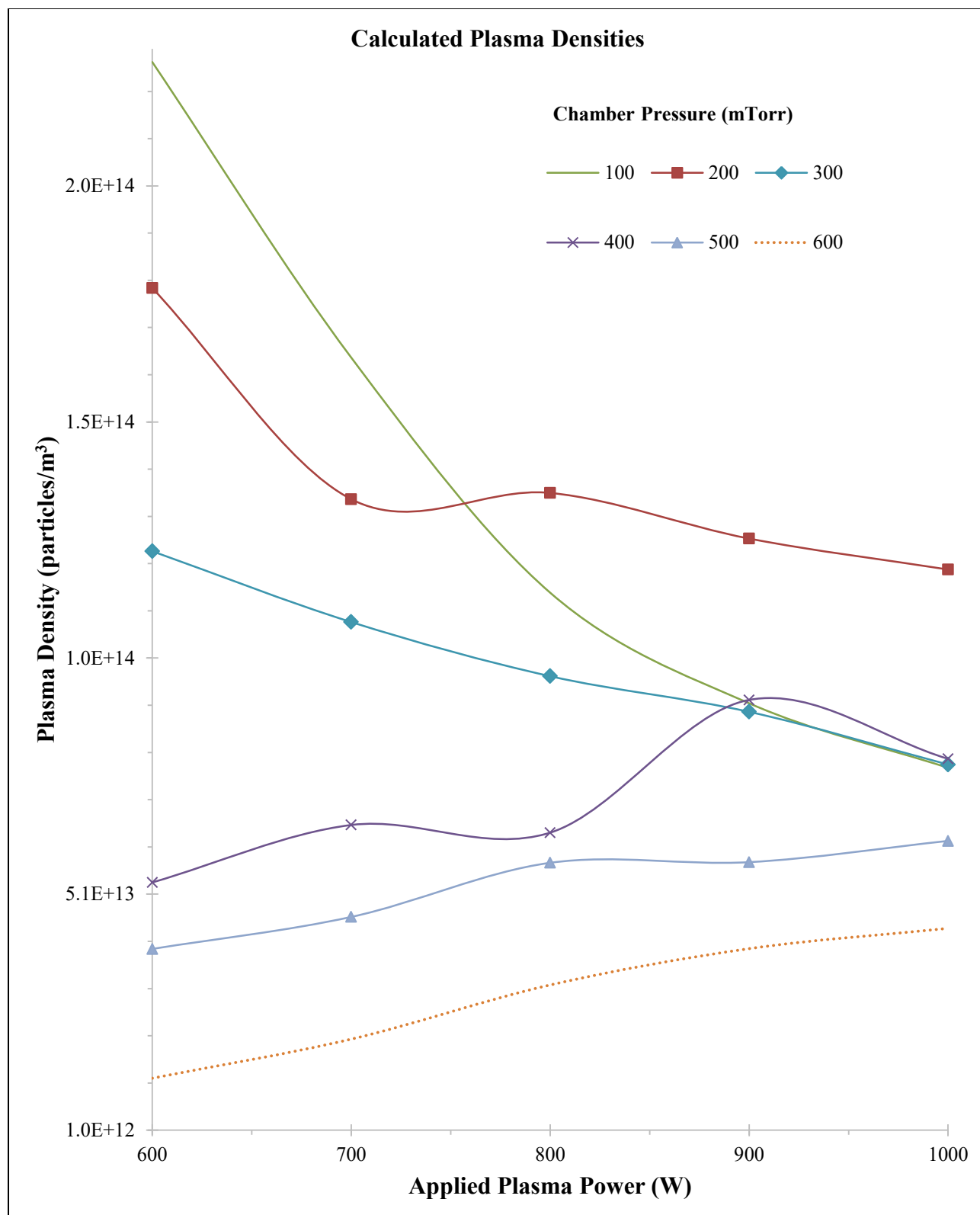


Figure 18: Calculated Plasma Densities from Langmuir Probe Measurements

From the collected and calculated data it is evident that varying the chamber pressure has a significant effect on the plasma characteristics. The applied plasma power setting and corresponding voltage supplied appears to have a lesser effect on plasma characteristics. However, a sufficient voltage must be supplied to ignite and maintain stable plasma. It is shown in Figure 17 and Figure 18 that increasing the chamber pressure has the most impact on the plasma at lower pressures, as seen from the data from 100 – 300mTorr. Varying the applied plasma power appears to only significantly affect the plasma temperatures and densities at lower pressures, seen in the data collected at 100mTorr.

As the chamber pressure is increased from 200 – 600mTorr, both the electron temperature and plasma density generally decrease. Increasing the applied plasma power and corresponding applied voltage results in an electron temperature increase. It was generally observed that as the applied plasma power was increased at lower chamber pressures, from 100 – 300mTorr, the plasma density decreases and when increased at higher pressures, from 400 – 600mTorr, the plasma density increases.

With an understanding of these trends and knowing the plasma compositions from the spectroscopic data, chamber conditions can be selected to provide more favourable conditions for III-N crystal growth. Chamber parameters may be selected that result in electron and ion temperatures low enough to avoid unwanted effects such as plasma etching while maximizing plasma density and atomic nitrogen content for example.

It was observed that the actual plasma power is not always able to reach the applied plasma power specified. The actual plasma power achieved was also observed to decay as the plasma was run repetitively, as is required during growths.

4 Experimental Growth Results

4.1 Growth Considerations and Procedure

It was found that chamber pressure is the variable parameter which affects plasma characteristics the most. Experimental growths were performed in order to investigate how the varying chamber pressures and the resulting plasma conditions affect III-N crystal growth. This was done by growing and analyzing various GaN samples with varying chamber pressures and all other growth conditions kept constant. The actual plasma powers achieved during growth were monitored and average plasma powers were considered when analyzing the results

Chamber pressures were varied from 200 – 450mTorr in 50mTorr steps with an applied plasma power set at 800W. A growth at a chamber pressure of 225mTorr with an applied plasma power of 800W was also performed as the peak atomic nitrogen production was observed at this pressure. All samples were grown on $\approx 1\text{cm} \times 1\text{cm}$ sapphire substrates which were rinsed in acetone immediately prior to growth to prevent possible surface contamination. The substrate holder rotates at 60 rpm during growth to promote uniform material deposition. Each growth cycle consists of a 4 second TMGa precursor pulse followed by an 8 second plasma pulse.

The growth procedure for all samples can be summarized as follows:

- The sapphire substrate is cleaned and immediately placed into the growth chamber.
- The growth chamber is gradually heated over 30 minutes.
- A GaN buffer layer consisting of 100 cycles is grown at a lower temperature than the subsequent growth layers, $\approx 640^\circ\text{C}$.
- A GaN layer consisting of 900 growth cycles is grown at $\approx 700^\circ\text{C}$.
- The sample is allowed to cool while still under vacuum in the growth chamber.

The actual average plasma powers observed during growth for all samples are shown in Figure 19. As can be seen, although the applied plasma power was held constant for all growths, the actual plasma power achieved varied significantly as the chamber pressure was varied.

The initially achieved plasma powers at the beginning of the growths were observed to be roughly 100 – 200W higher than the stabilized values. The gradual decrease in achieved powers before stabilizing was found to take roughly 100 – 150 growth cycles. This variance in plasma power as the growth progresses is another factor likely contributing to the resulting overall quality of the growths.

The calculated electron temperatures, plasma densities, and measured atomic nitrogen peaks taken at 745nm with an applied plasma power of 800W are shown in Figure 20, Figure 21, and Figure 22 respectively. The resulting growths were analyzed and compared using various characterization techniques which are discussed in the following sections.

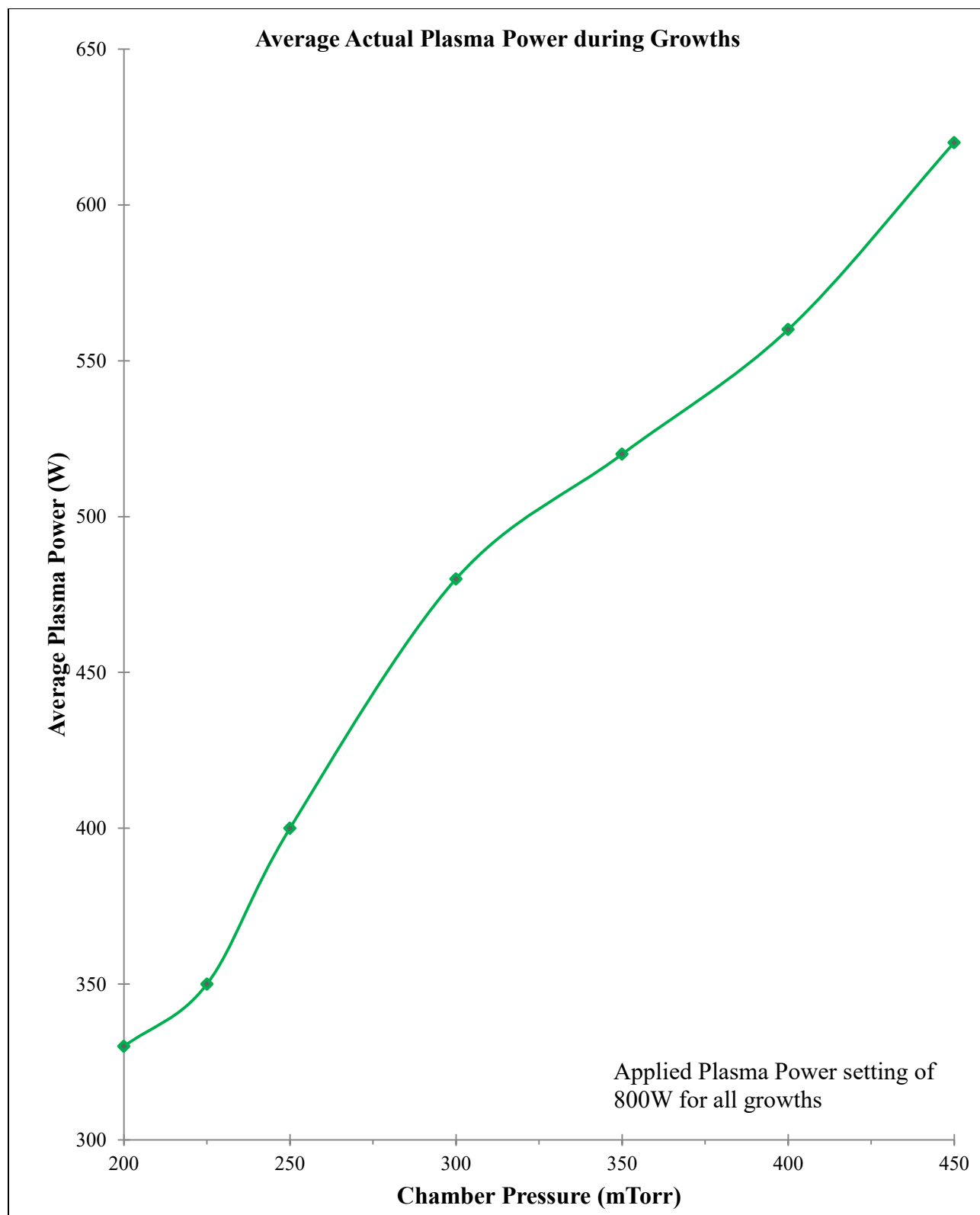


Figure 19: Average Actual Plasma Power during Growths

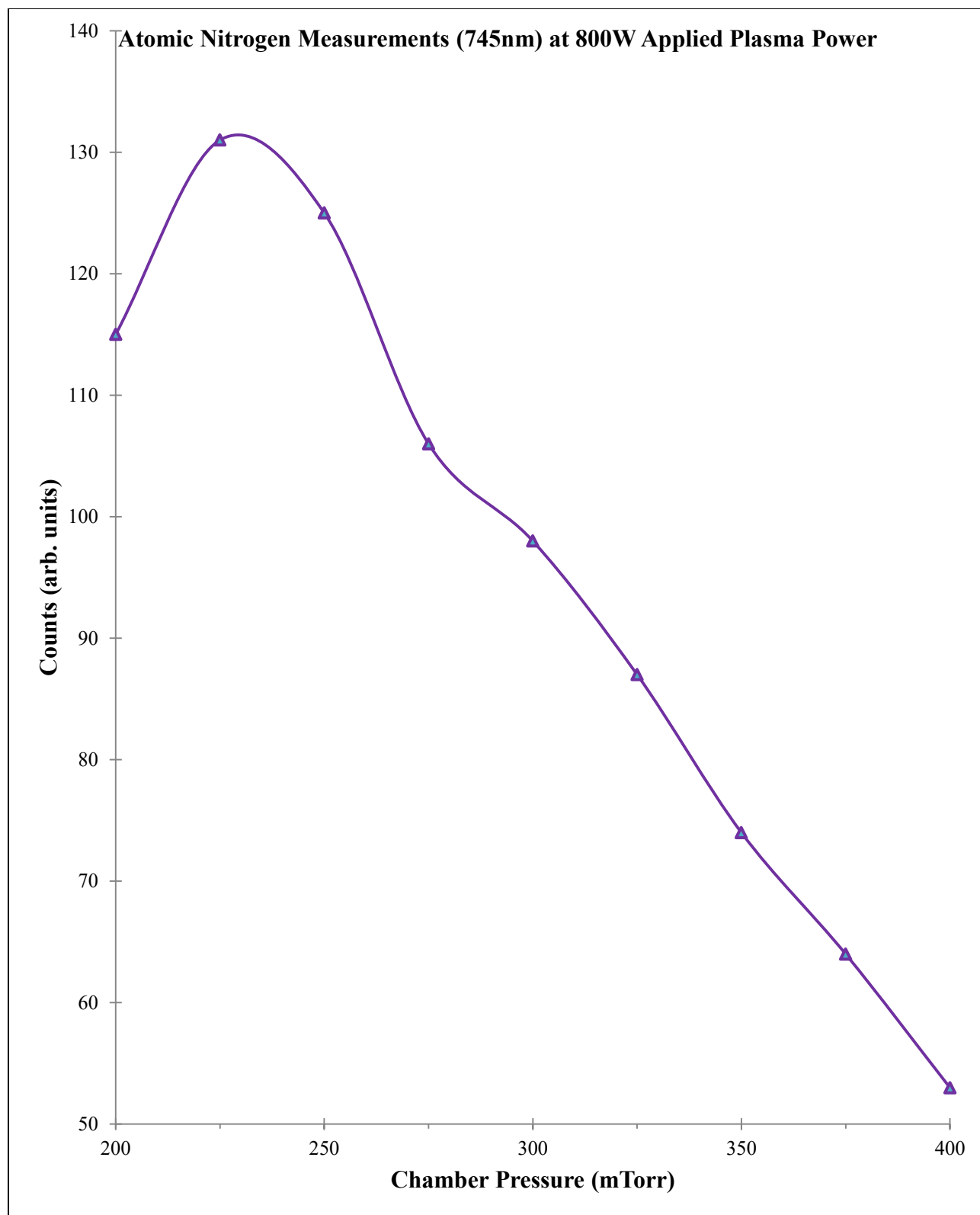


Figure 20: Atomic Nitrogen Measurements (745nm) at 800W Applied Plasma Power

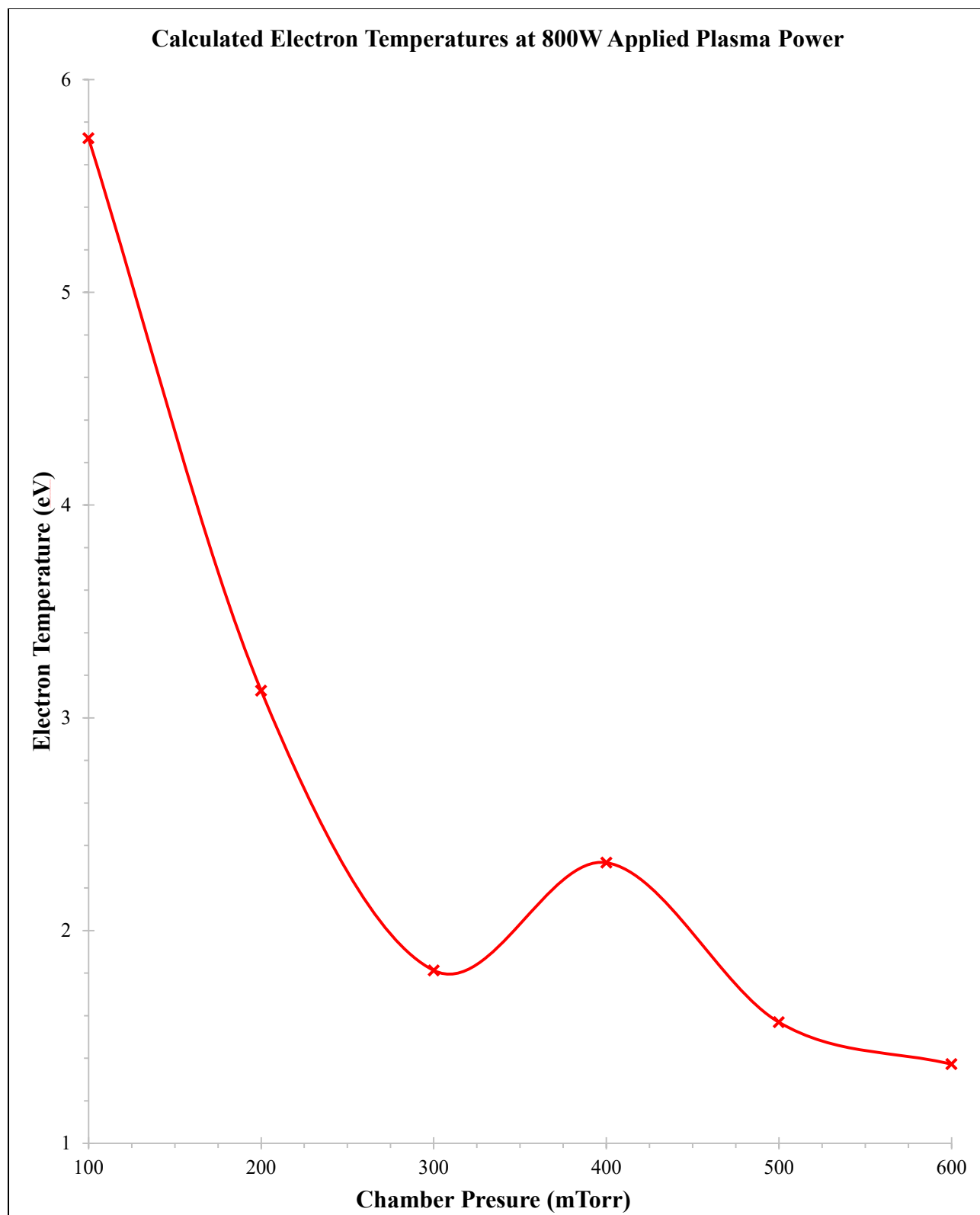


Figure 21: Calculated Electron Temperatures at 800W Applied Plasma Power

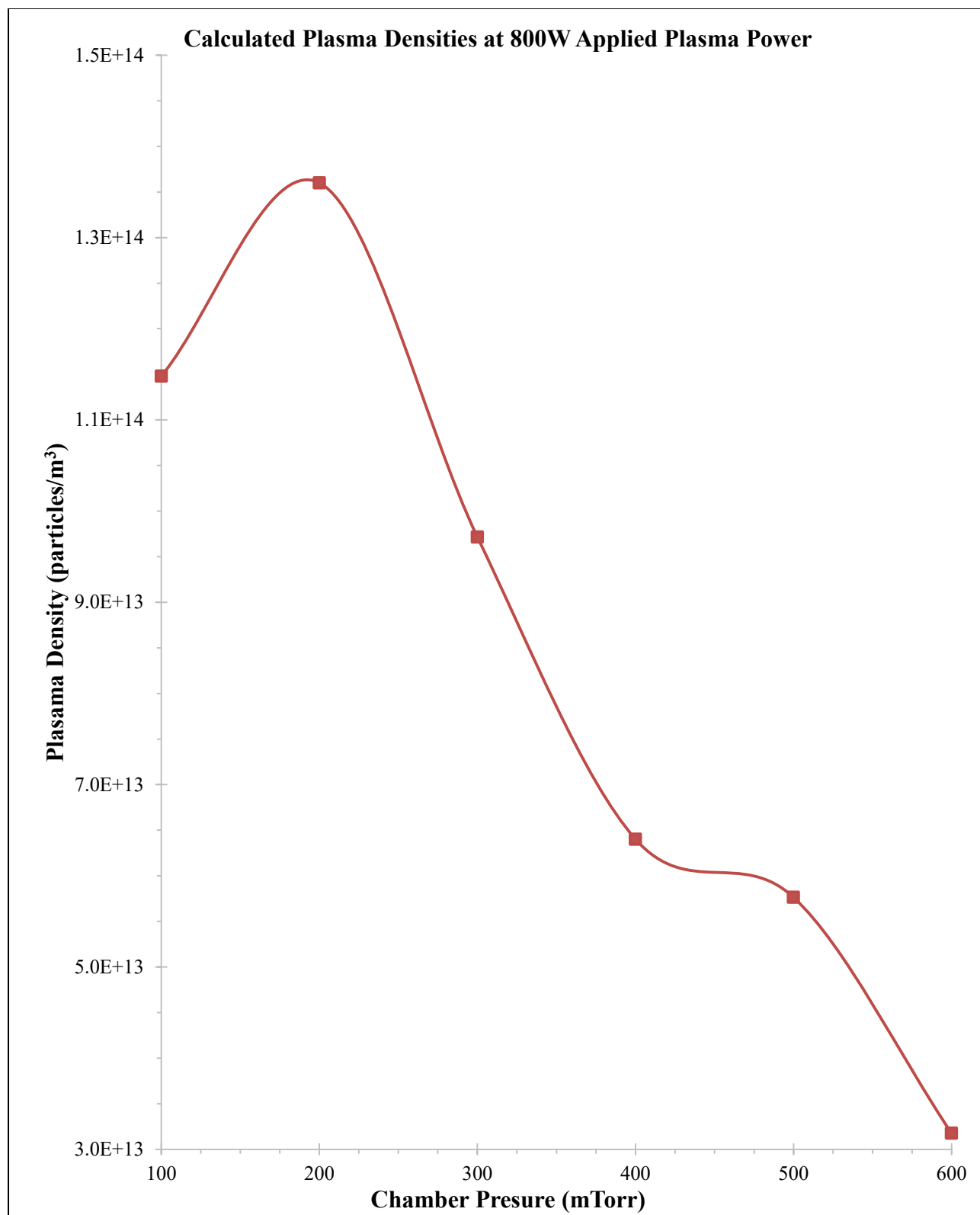


Figure 22: Calculated Plasma Densities at 800W Applied Plasma Power

4.2 Characterization Techniques and Results

4.2.1 X-Ray Diffraction

The first characterization method considered to determine if crystalline growth in the desired orientation has occurred and to analyze crystalline growth quality is X-ray diffraction (XRD). As depicted in Figure 23, X-rays with a set wavelength, λ , are directed at the sample from a wide range of angles.

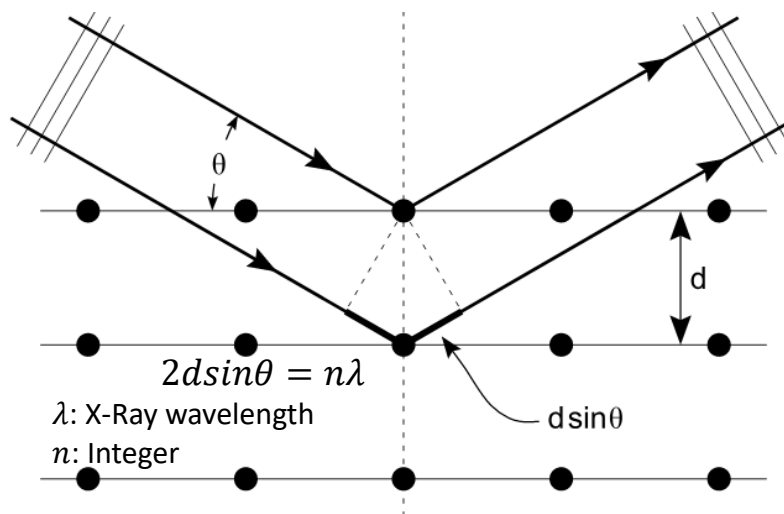


Figure 23: Bragg Diffraction [14]

Photons with wavelengths on the scale of the sample atomic lattice distances, d , are required to produce constructive interference patterns, this requires X-rays. Scattered photons from the electron clouds surrounding the periodically spaced atoms in a crystalline sample produce constructive interference patterns and are detected and measured [15]. These conditions fulfil the requirements for Bragg diffraction and Bragg's law can be used to determine the interplanar atomic lattice distances of the sample using the following expression.

$$2d \sin \theta = n \lambda \quad (4)$$

With the atomic lattice spacing for specific compounds known, the resulting measurements from the sample can be compared and the growth orientation and the degree of crystallinity can be determined.

For the characterization of the experimental growths a PANalytical X'Pert Pro MRD X-ray diffractometer performing $\theta/2\theta$ scans was used. During a $\theta/2\theta$ scan the sample sits on a fixed stage as the X-ray source and detector are kept at a fixed, normal angle towards the sample and are rotated through angles θ at a constant specified rate. The X-ray source in this diffractometer is a copper anode in a vacuum tube. The copper target is bombarded by high-energy electrons which result in X-ray emissions as electrons transition from a higher to lower orbital level due to atomic interactions. The X-ray emission relevant for these measurements is the $k\text{-}\alpha_1$ emission, resulting from an electron falling from the L to K electron shell level, having a wavelength of 0.1540598 nm. The tube current was set at 40mA and the accelerating voltage at 45kV.

XRD measurements were performed on all experimental growth to determine wurtzite GaN growth crystallinity in the desired [002] orientation, known to be found at $2\theta = 34.632^\circ$. Deviations in the measured peaks from this location are indicative of strains or other defects on the growths which results in shifting of the interplanar atomic lattice distances [15].

The results for the four growths showing the highest growth crystallinity in are shown in Figure 24. Results for the growths performed at 225, 250, and 300mTorr are shown in Figure 25. No crystalline GaN growth was found on the sample grown at 200mTorr.

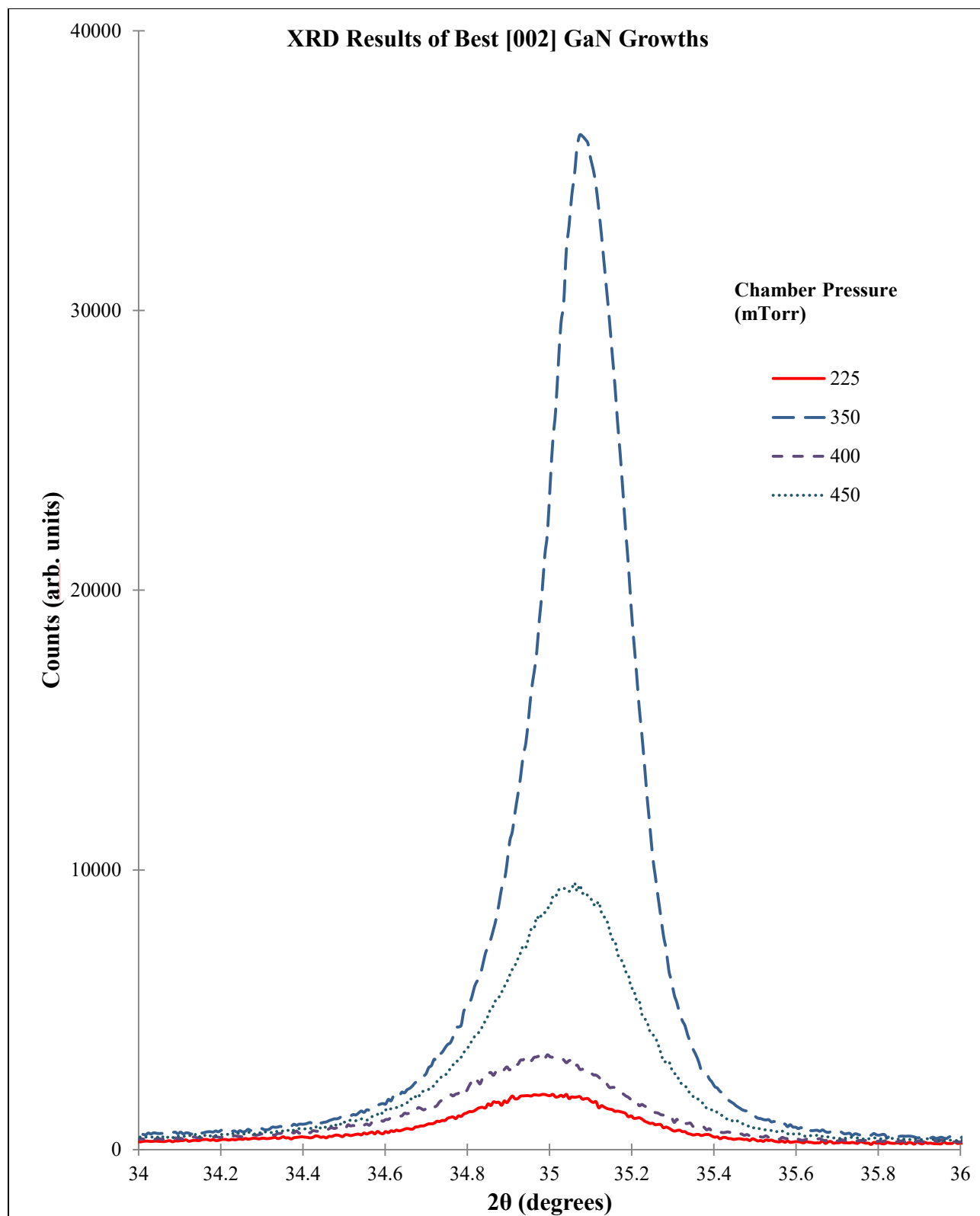


Figure 24: XRD Results of Best GaN Growths

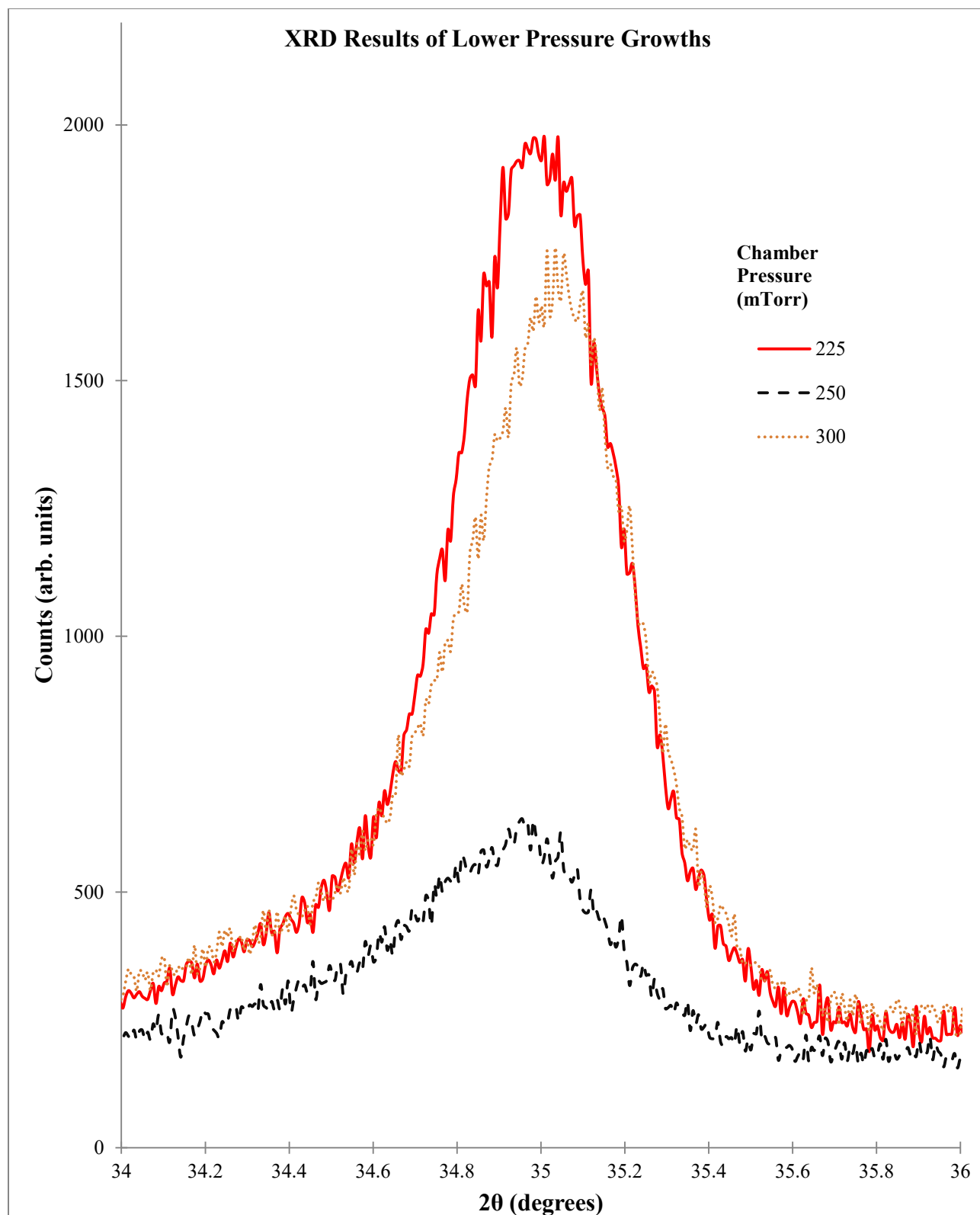


Figure 25: XRD Results of Lower Pressure GaN Growths

From Figure 24 it is apparent that although at 225mTorr the highest atomic nitrogen emissions were measured, the growth performed at this pressure did not produce the most crystalline GaN layer. The four best growths, in order of decreasing desired crystallinity, were found to occur at chamber pressures of 350, 450, 400 and then 225mTorr. The growths at 250 and 300mTorr were found to be of lesser crystallinity than that for the growth at 225mTorr, as can be seen in Figure 25.

An explanation as to why growths from pressures of 350 – 450mTorr produce the most crystalline GaN layers is that it may be due to the higher average plasma powers, seen in Figure 19, than those found at lower pressures. It is hypothesized that these higher plasma powers could be possibly encouraging crystal growth as more energy is supplied to the system.

The lower plasma temperatures found at these higher chamber pressures, shown in Figure 21, could also be reducing any potential etching effects which may be occurring at lower pressures.

The previously observed trends of how varying the chamber pressure affects available atomic nitrogen also must be considered. From the recorded spectroscopic data the atomic nitrogen emissions were found to decrease as chamber pressures increased beyond 225mTorr. The trend seen in Figure 22 shows that increasing chamber pressure results in a decrease in plasma density, also reducing the amount of available atomic nitrogen species as seen in Figure 20. This may contribute as to why the growth at 350mTorr produced better results rather than those at higher pressures.

4.2.2 Atomic Force Microscopy

Atomic force microscopy (AFM) is a relatively simple and fast characterization technique which allows for the investigation of surface characteristics of samples at an atomic-scale resolution. A block diagram depicting the principles of AFM operation is seen in Figure 26.

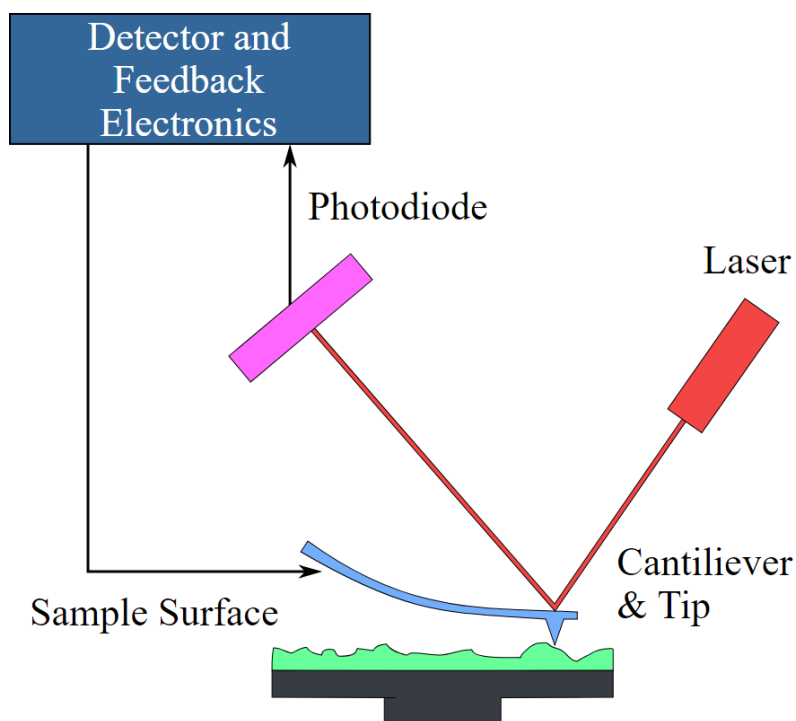


Figure 26: AFM Operating Principle [16]

AFM measurements are performed as a very fine-tipped probe drags along or scans very close to a sample surface. There are three possible measurement modes called contact, non-contact, and tapping mode. A laser feedback system monitors the height variations of the probe tip at evenly spaced points and an image of the sample surface can be produced.

In non-contact mode the probe tip oscillates at a resonant frequency and is brought close enough to a sample for Van der Waals, electrostatic, and others forces to affect the oscillation as

it scans along the surface. As these forces variably affect the oscillation as surface height varies, a controller shifts the height of the probe to maintain the resonant frequency.

In contact mode the probe tip drags along the sample surface and the resulting static deflection is monitored. As the degree of deflection varies, the probe height is varied to keep the forces acting on the tip constant. As the radiuses of the tips used are on the scale of tens of nanometers and therefore quite fragile, this mode leaves the tips susceptible to damage, especially for rough samples.

Tapping mode is similar to non-contact mode but the probe is kept at a height to maintain a constant force on the tip. This may result in the probe tip coming into contact with the sample resulting in wear on the tip and potentially being damaged or broken.

AFM measurements were performed on the growths using a AFM Nanosurf Easyscan 2 operating in non-contact mode using silicon ACL-A probes featuring a tip radius of less than 10nm. There were 512 measurements points per line with a scan rate of 1second per line.

The result for the growth performed at 350mTorr, measured to have the most crystallinity, is shown in Figure 27 with a measured RMS surface roughness of 3.956nm. The growth at 225mTorr, the pressure where peak atomic nitrogen emissions occur, is shown in Figure 28 with a measured RMS surface roughness of 1.184nm.

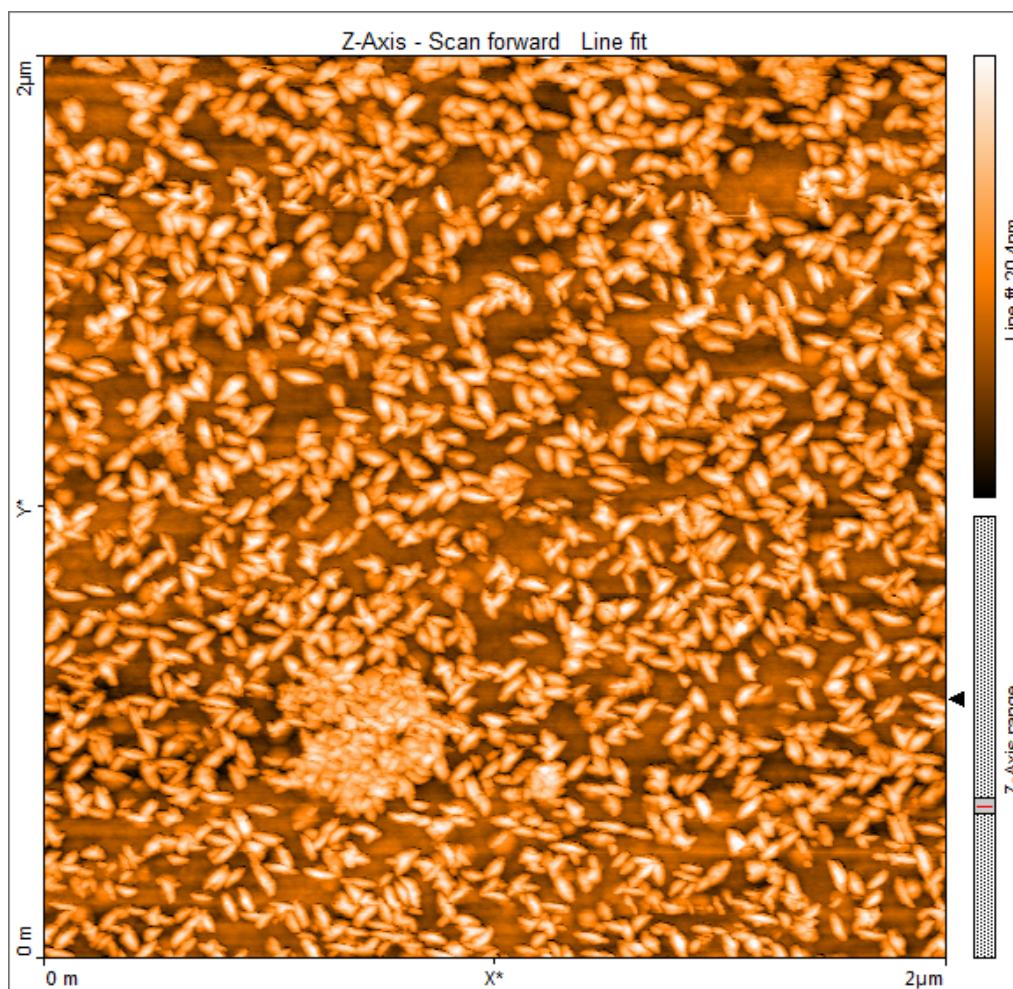


Figure 27: AFM Result for Growth at 350mTorr, 800W (2µm x 2µm)

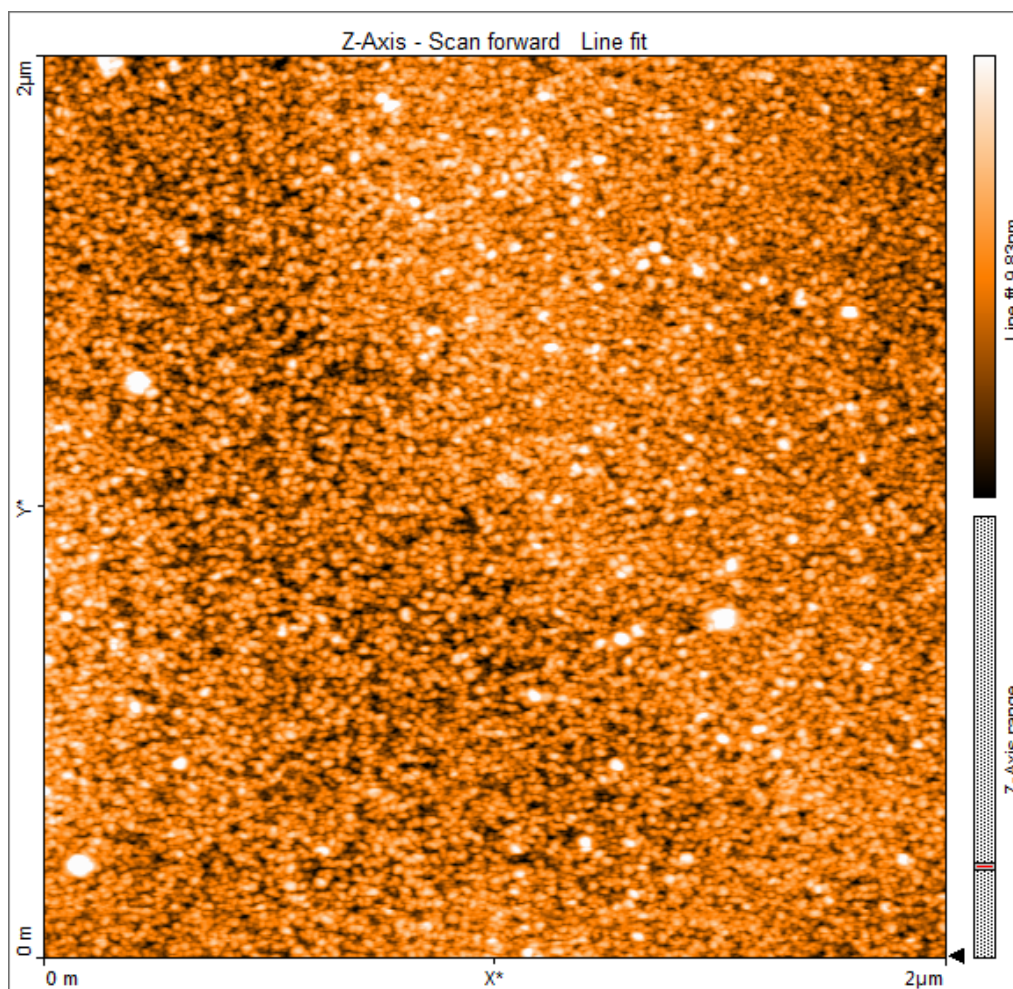


Figure 28: AFM Result for Growth at 225mTorr, 800W (2 μ m x 2 μ m)

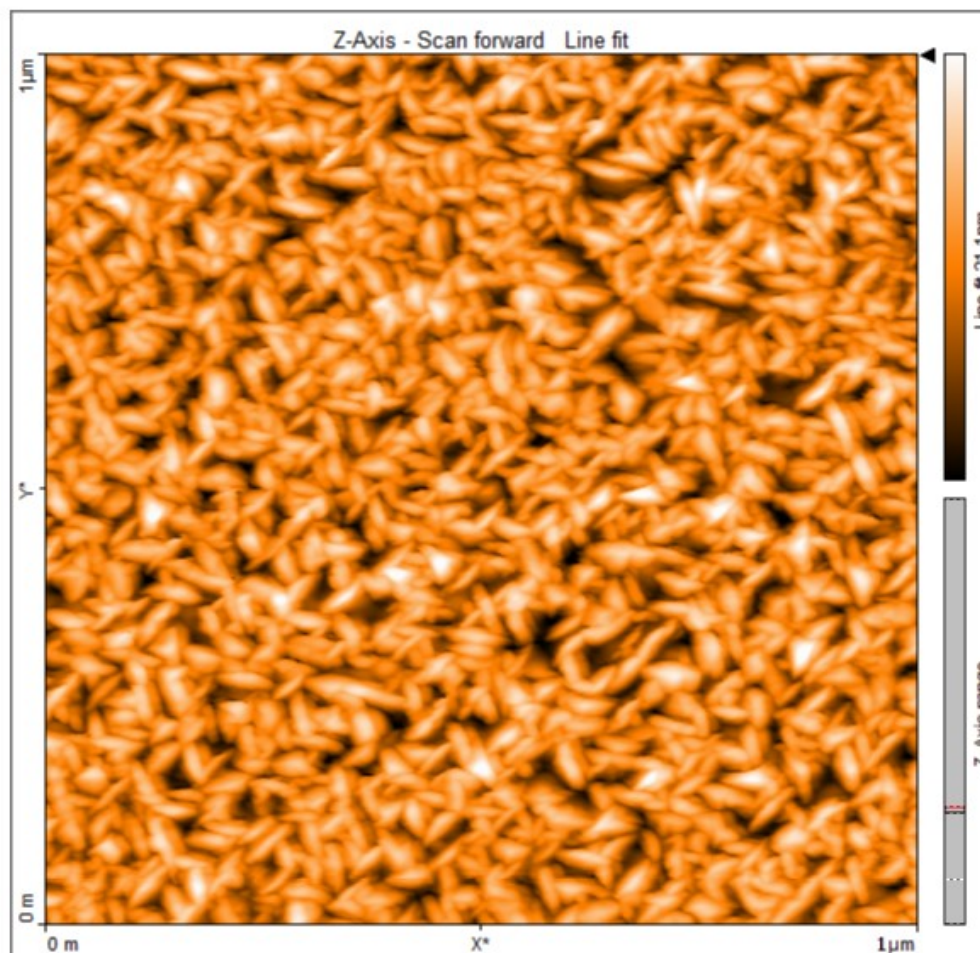


Figure 29: AFM Result for Growth at 450mTorr, 800W (1 μm x 1 μm)

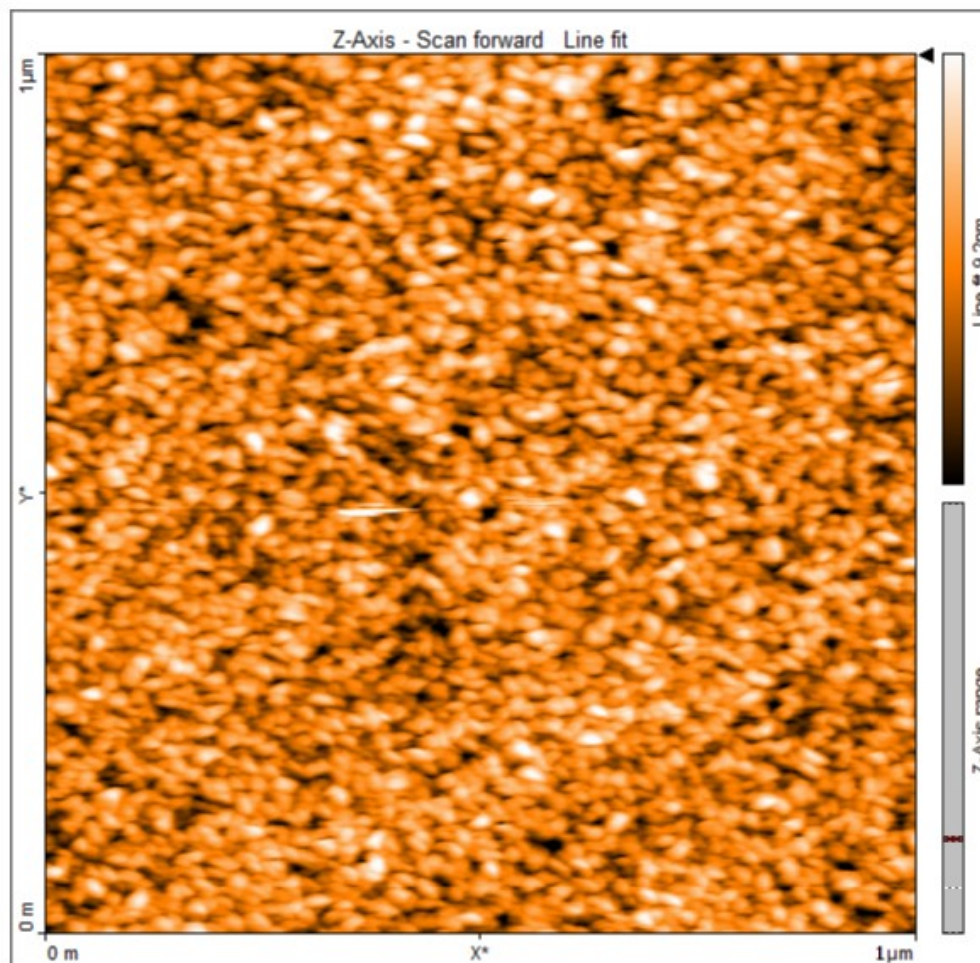


Figure 30: AFM Result for Growth at 300mTorr, 800W (1 μm x 1 μm)

AFM results for the growths performed at chamber pressures from 350 – 450mTorr all show similar elongated particles formations as seen in Figure 27. These formations became more densely distributed as the chamber pressure increased as seen from the AFM result for the growth at 450mTorr, shown in Figure 29 which was found to have an RMS surface roughness of 3.514nm. The RMS surface roughnesses for these higher pressure growths range from 2 – 4nm.

The AFM results for the growths performed at pressures from 200 – 300mTorr all show a similar smooth, uniform surface as seen in Figure 28. The RMS surface roughnesses for these lower pressure growths range from 1 – 1.6nm.

Comparisons with these AFM results for the lower pressure growths and the results showing declining crystallinity observed from the growths at 225, 300, 250mTorr and then no measured peaks at 200mTorr may be indicative of a combination of etching and the atomic nitrogen content affecting the growths. The observed smooth, uniform surfaces occurring on the growths at lower chamber pressures and the presence of particle formations on the higher pressure growths further suggests that plasma etching is occurring at lower pressures. It appears that the higher atomic nitrogen content at 225mTorr does noticeably contribute positively towards growth but the plasma temperature is a more dominant factor as seen by the further indications of etching from the AFM results.

The required minimum chamber pressure which results in plasma temperatures low enough to avoid plasma etching appears to be near 350mTorr. This is based on the AFM results showing particle formations on the surface and peak crystallinity measured from the growth performed at 350mTorr and comparing this with the indications of plasma etching seen at 300mTorr, shown in Figure 30 where an RMS surface roughness of 1.506nm was measured.

4.2.3 Scanning Electron Microscopy

Scanning electron microscopy (SEM) is another surface imaging technique where a focused electron beam is scanned along a sample and allows the surface of the sample to be observed and measurements made at an atomic-scale resolution. The incident electron beam causes electrons from the sample surface to be ejected or backscattered which are then detected. These resulting measurements allow for an image to be produced and information regarding the sample, such as layer thickness and chemical composition, to be investigated.

As opposed to the relatively simple AFM imaging technique, SEM measurements require prior sample preparation. Measures must be taken to ensure that the sample is conductive, allowing a path to ground for the electrons. A scanning electron microscope is also a much more complicated and expensive instrument. It is operated under deep-vacuum conditions at pressures in the range of $10^{-5} - 10^{-7}$ Torr, increasing the free path lengths of electrons. A series of lenses is used to focus the electron beam as it is accelerated by a high voltage, on the scale of tens of kilovolts, towards the sample.

A schematic of a scanning electron microscope is seen in Figure 31. A depiction of the working principle of SEM and other available measurement techniques using this method is shown in Figure 32.

SEM images were taken of the experimental growths using a Hitachi SU-70 scanning electron microscope with an accelerating voltage of 10kV. A thin layer of carbon was sputtered onto the samples or a layer of carbon paste was applied prior to SEM measurements.

SEM images for the samples grown at 225 and 350mTorr from different orientations and magnifications are shown from Figure 33 to Figure 40.

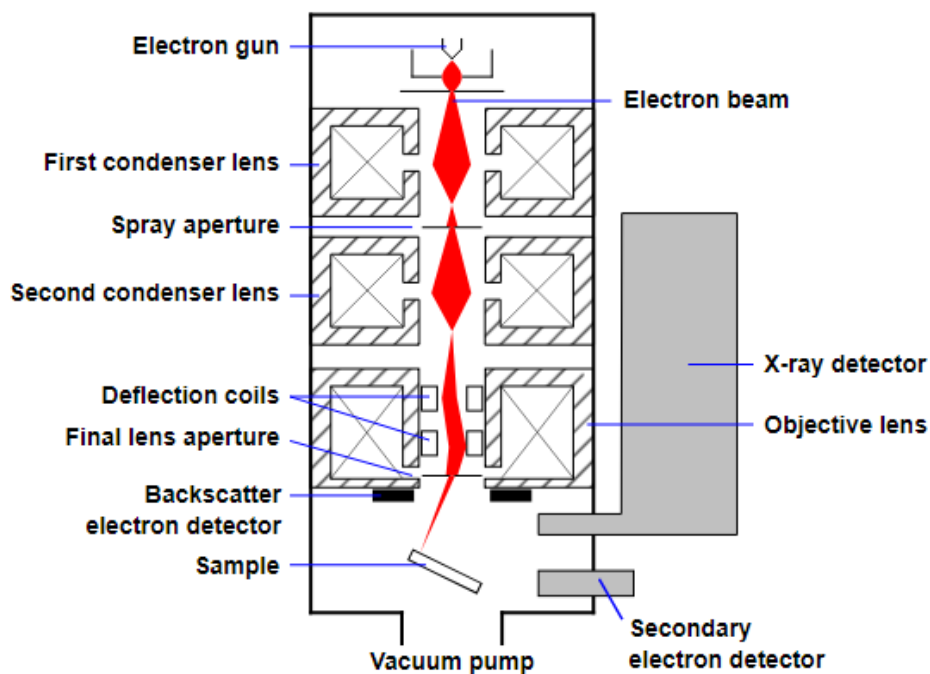


Figure 31: Schematic of a Scanning Electron Microscope [17]

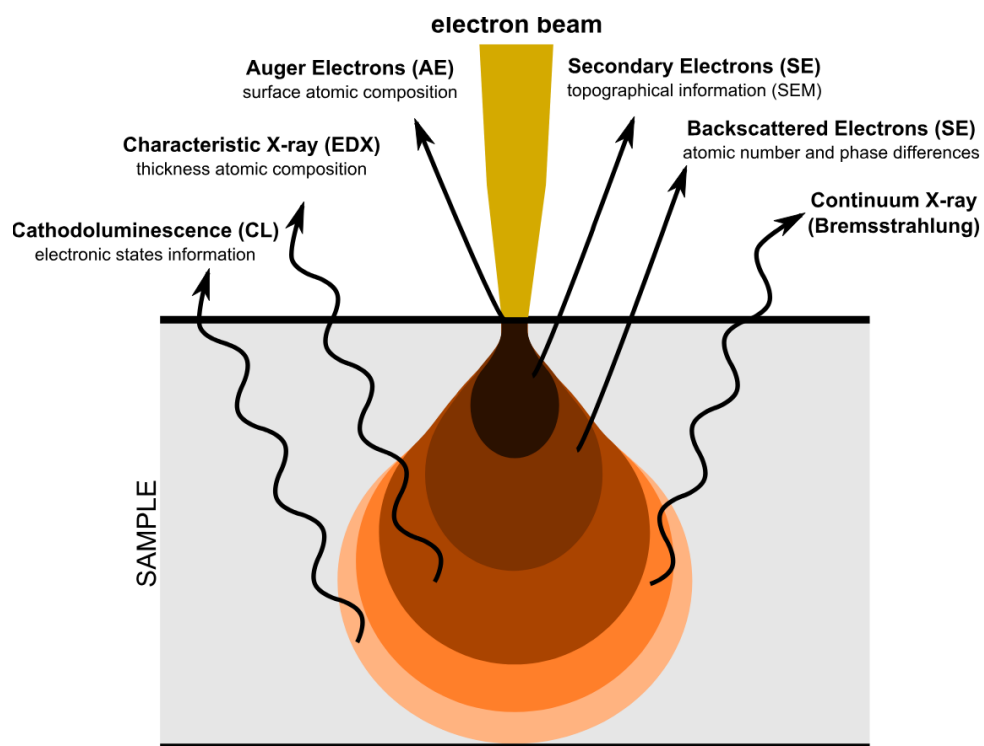


Figure 32: SEM Operating Principle [18]

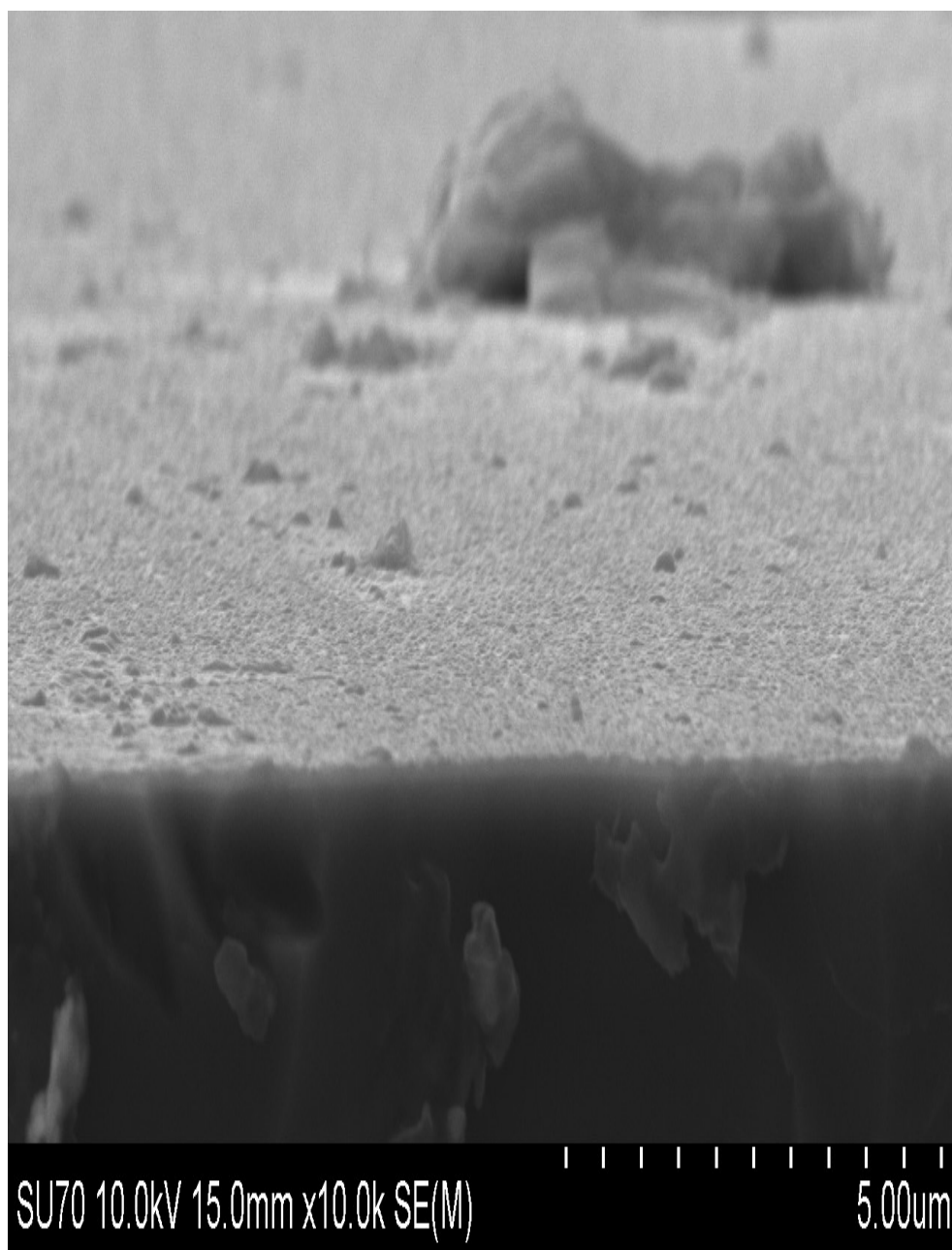


Figure 33: SEM Surface-View of GaN Growth at 350mTorr, 800W



Figure 34: SEM Surface-View of GaN Growth at 225mTorr, 800W

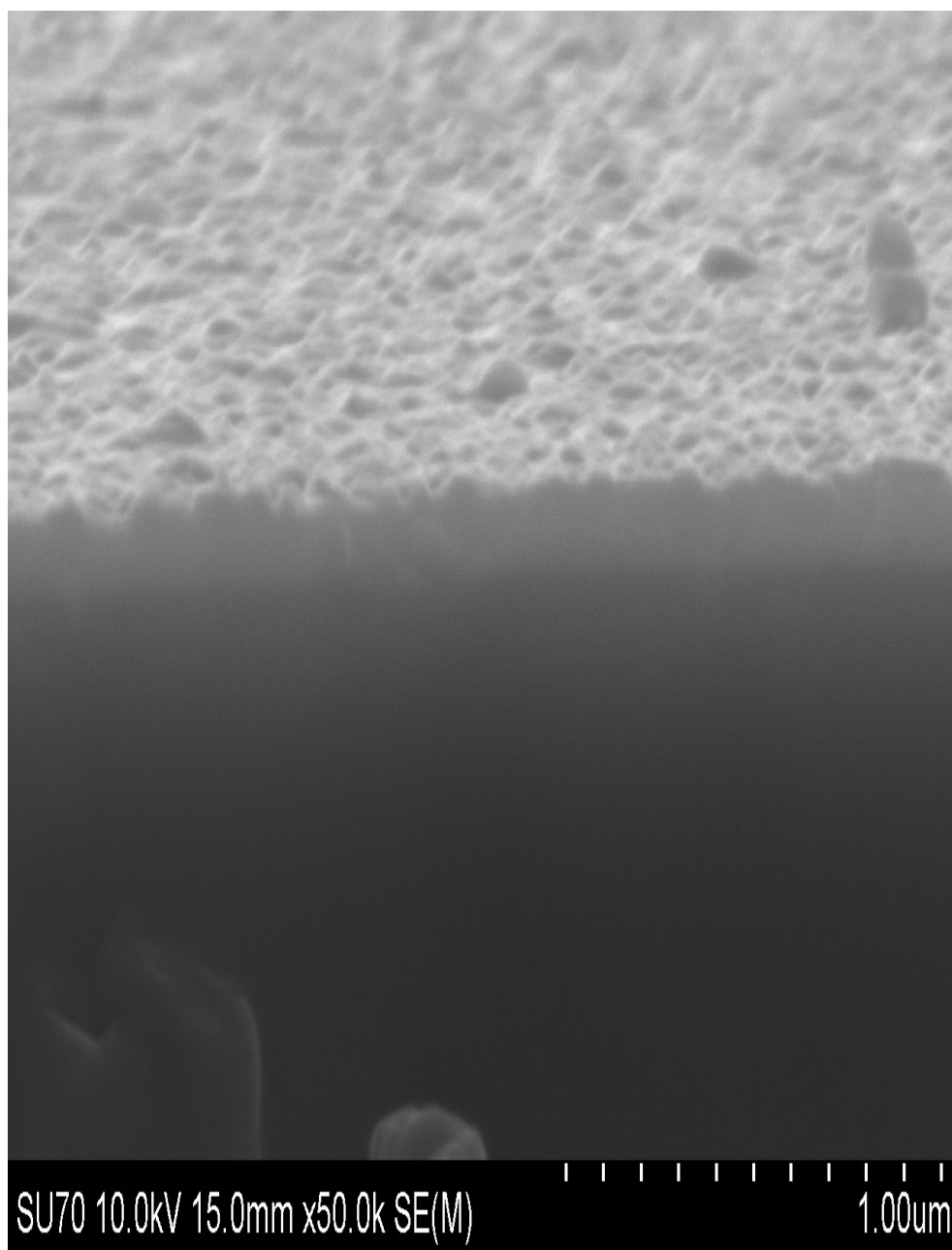


Figure 35: SEM Surface-View of GaN Growth at 350mTorr, 800W with Increased Magnification

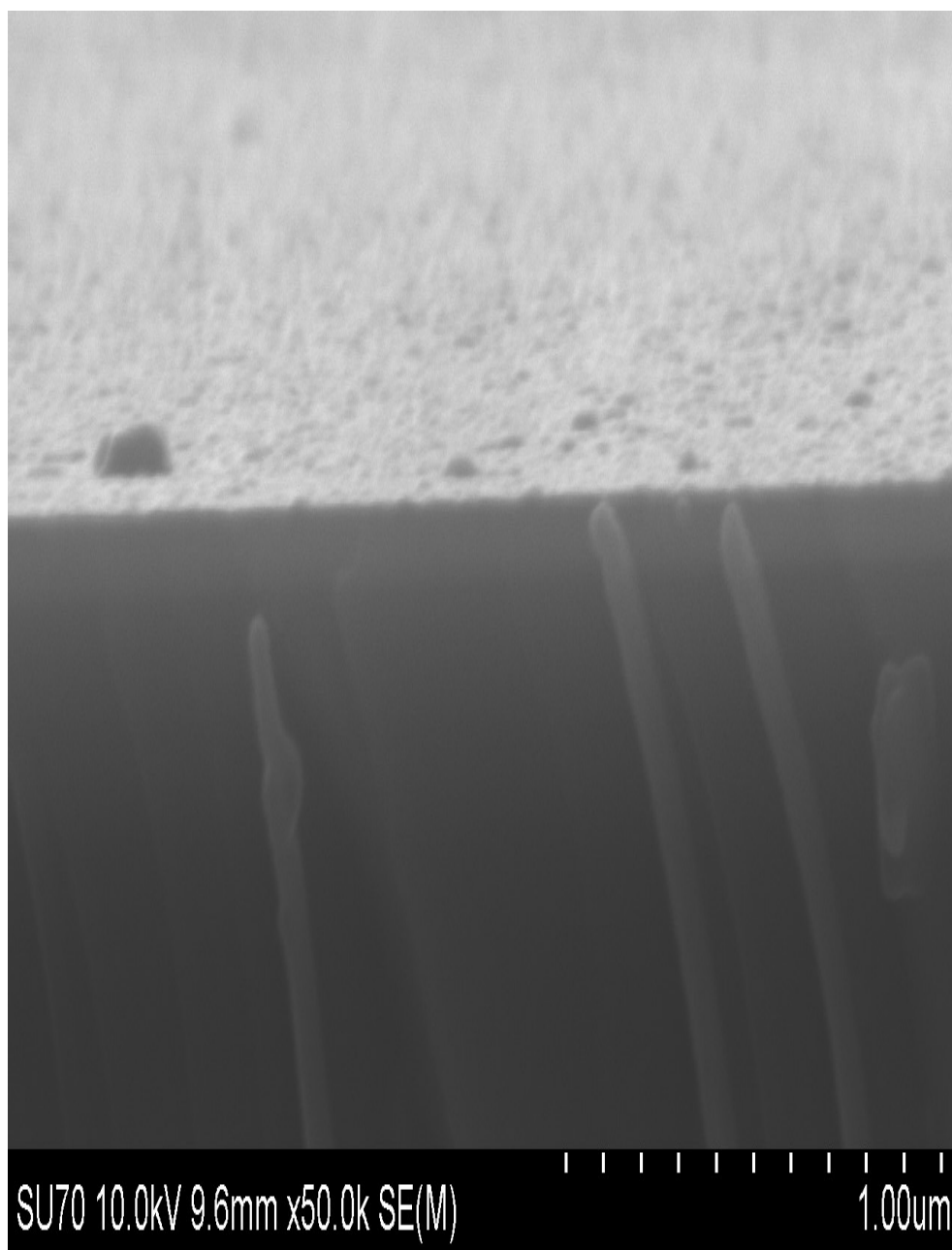


Figure 36: SEM Surface-View of GaN Growth at 225mTorr, 800W with Increased Magnification

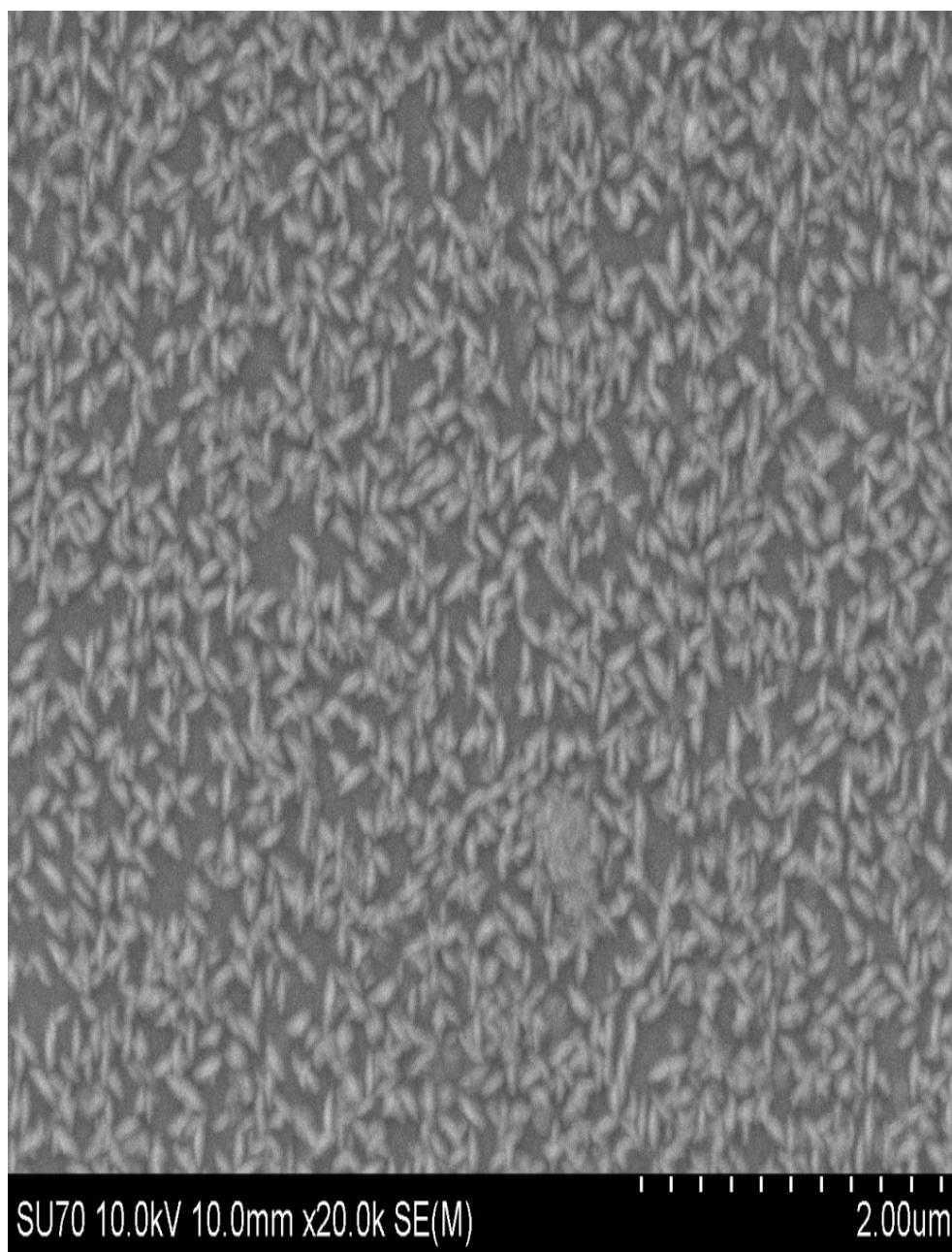


Figure 37: SEM Top-View of GaN Growth at 350mTorr, 800W

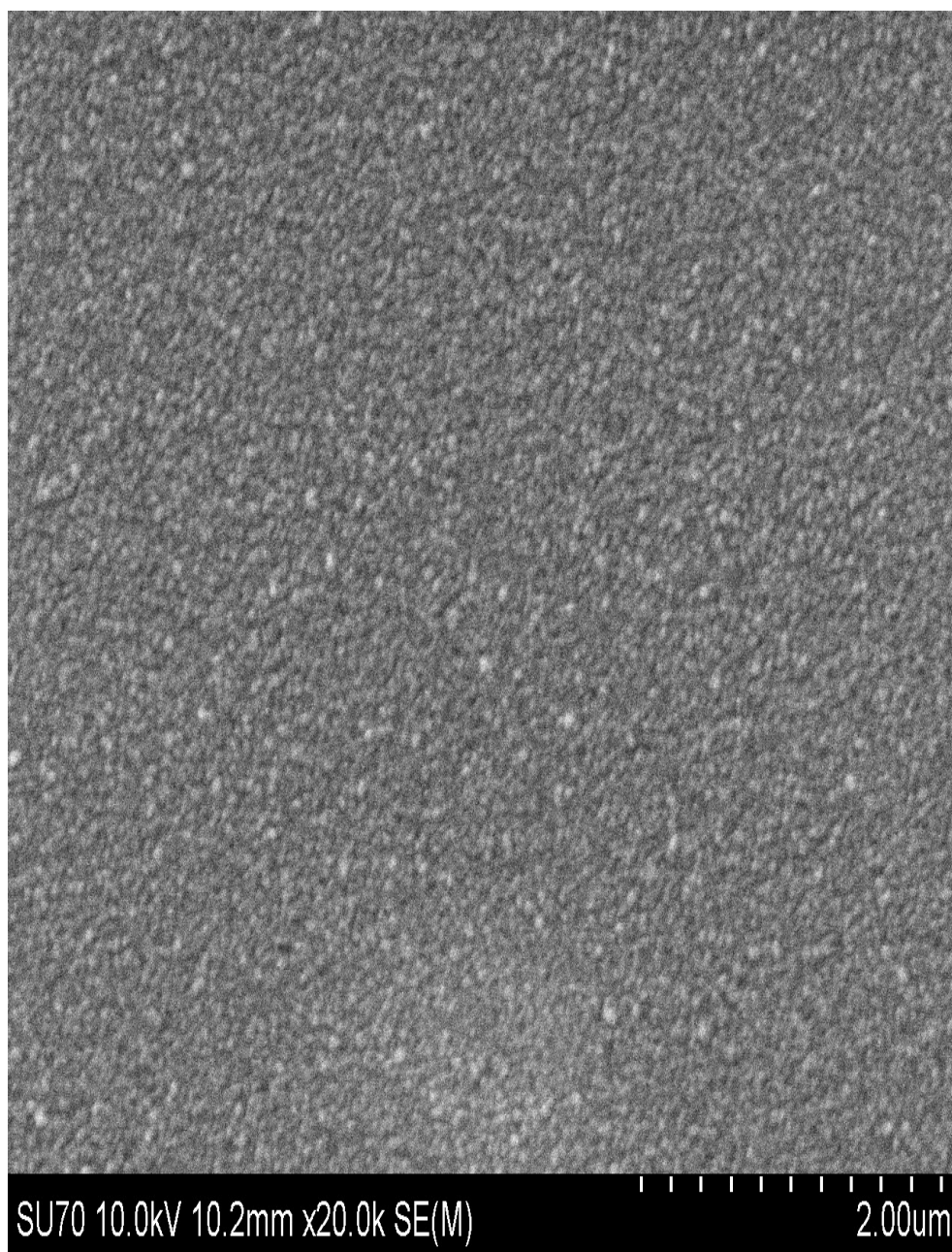


Figure 38: SEM Top-View of GaN Growth at 225mTorr, 800W

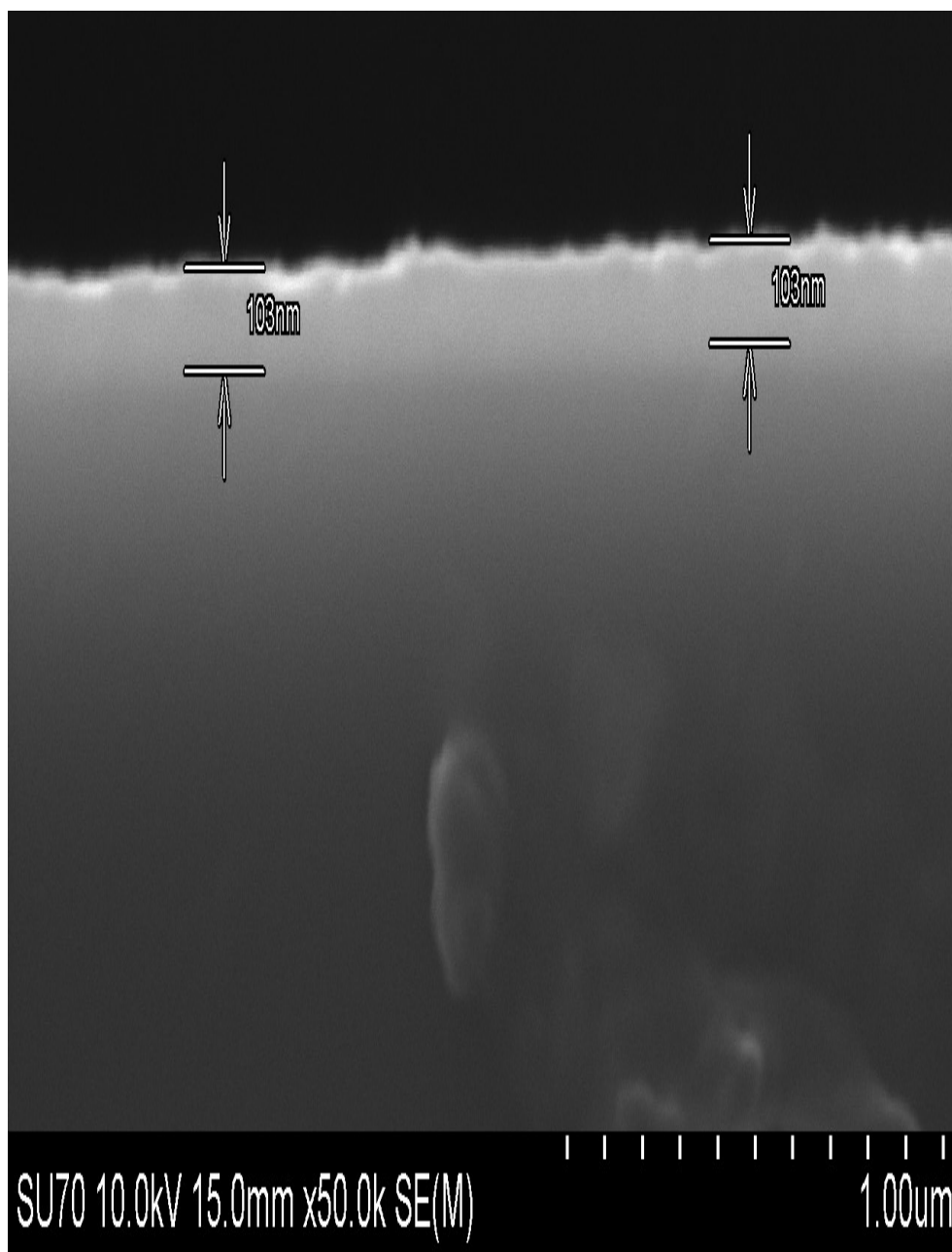


Figure 39: SEM Cross-Section of GaN Growth at 350mTorr, 800W

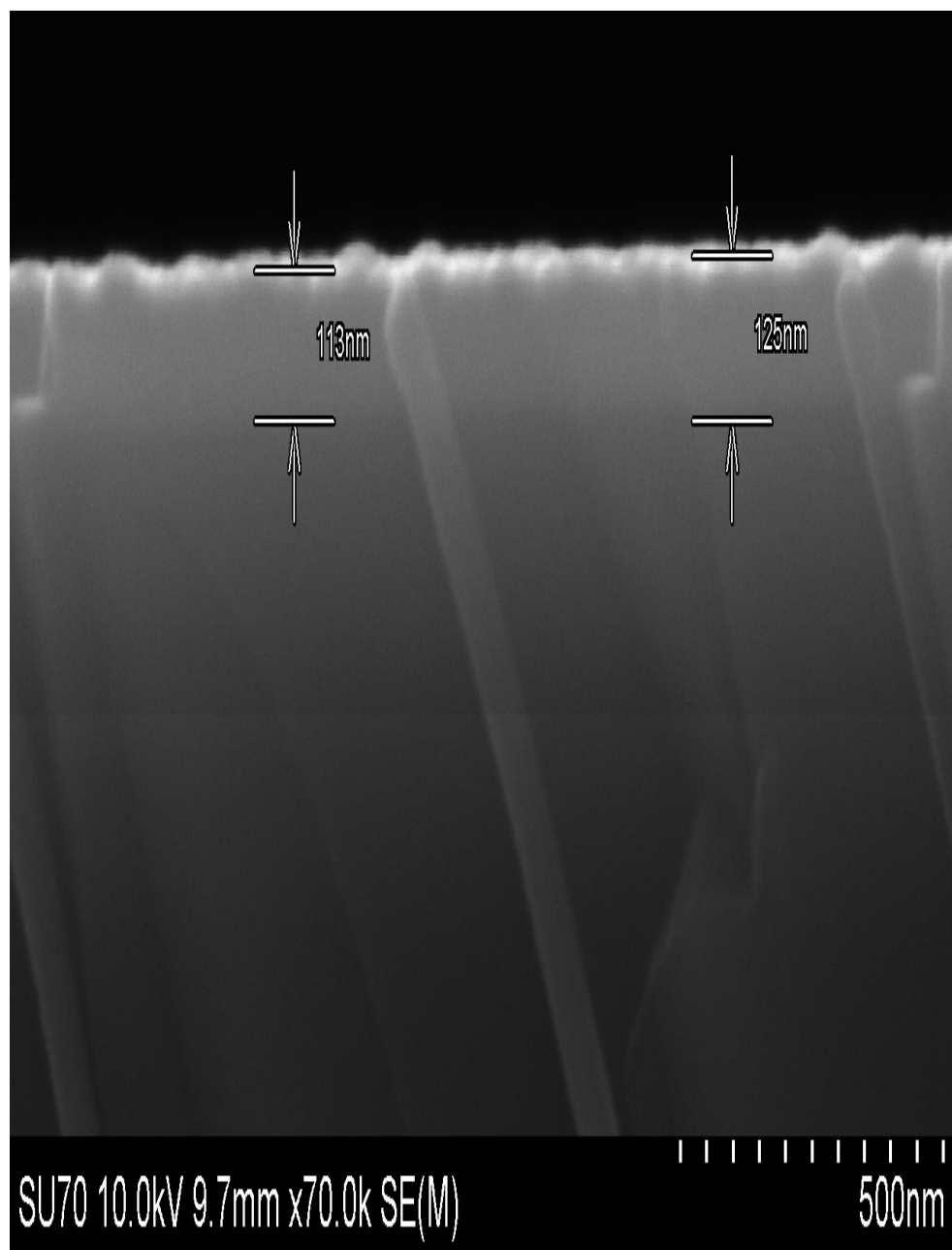


Figure 40: SEM Cross-Section of GaN Growth at 225mTorr, 800W

Seen in Figure 33 and Figure 34 are scattered, large clumps of material found on the surface of the growth performed at a chamber pressure of 350mTorr and small clumps of material found on the surface of the growth performed at 225mTorr. Seen in Figure 35 and Figure 36 are images of the growth surfaces taken with an increased magnification. It can be seen that the overall surface on the 350mTorr growth is rippled and rough whereas the 225mTorr growth has an overall smooth surface.

The presence of large clumps of material at higher pressures provides further evidence that the deposited material may possibly be getting ejected from the growth surface due to the higher plasma temperatures at the lower chamber pressures seen in Figure 21.

The top-down view of the sample surfaces, shown in Figure 37 and Figure 38, show elongated particle formations found on the 350mTorr growth and a more uniform, smooth surface for the 225mTorr growth. This closely resembles the AFM results for these samples as expected.

The cross-sectional views of these samples are shown in Figure 39 and Figure 40. The growth layer can be differentiated from the substrate as can be seen by the layers of different contrast. The growth rates were found to be similar with a roughly 100 – 120nm thick uniform GaN layer found on each sample. It appears that the increased plasma densities, seen in Figure 22, and the higher atomic nitrogen content, seen in Figure 20, at the lower pressures does not directly lead to a noticeably higher growth rate.

4.2.4 Energy-Dispersive X-Ray Spectroscopy

In conjunction with SEM imaging, energy-dispersive X-ray spectroscopy (EDX) measurements can be taken to determine the rough elemental composition of a sample. As shown in Figure 32, EDX measurements are made by directing a high-energy electron beam at a sample which results in the ejection inner-orbital electrons in a sample.

Depicted in Figure 41 and following the same emission mechanism as with XRD measurements, as an electron from a higher orbital level fills the resulting void, the difference in energy is ejected in the form of an X-ray and is detected. The amount of energy that is released is characteristic and specific for each element and the chemical composition of the material can be determined.

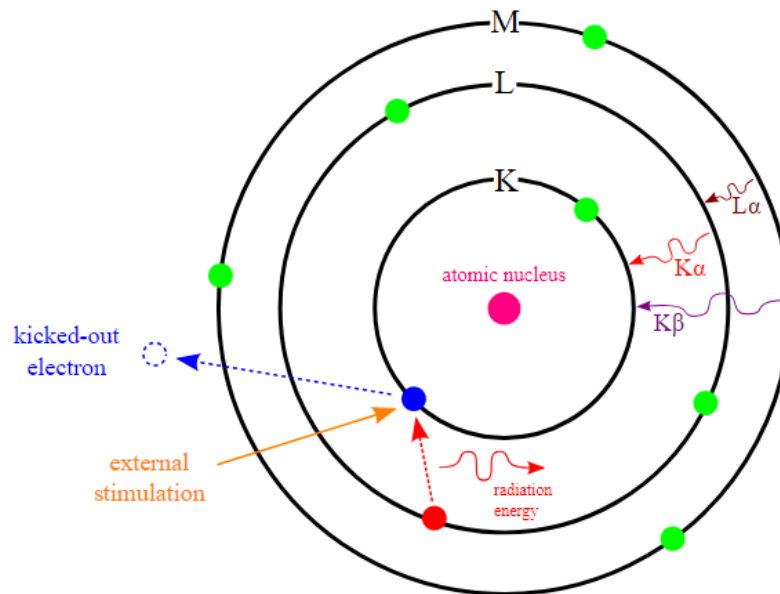


Figure 41: EDX Operation Principle [19]

The EDX results for the GaN layer for growths performed at 350mTorr and 225mTorr are shown in Figure 42 and Figure 43.

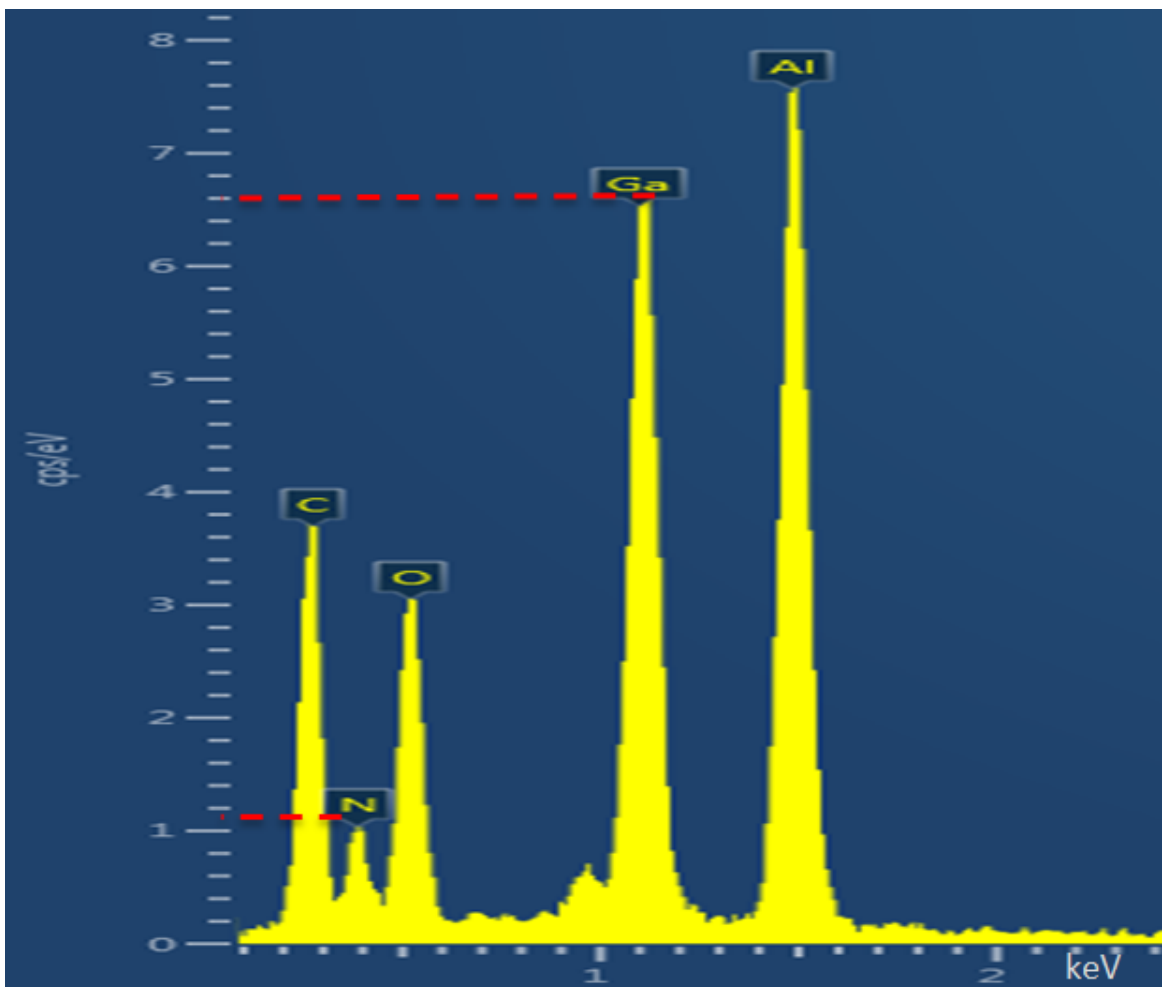


Figure 42: EDX Result for GaN Growth at 350mTorr, 800W

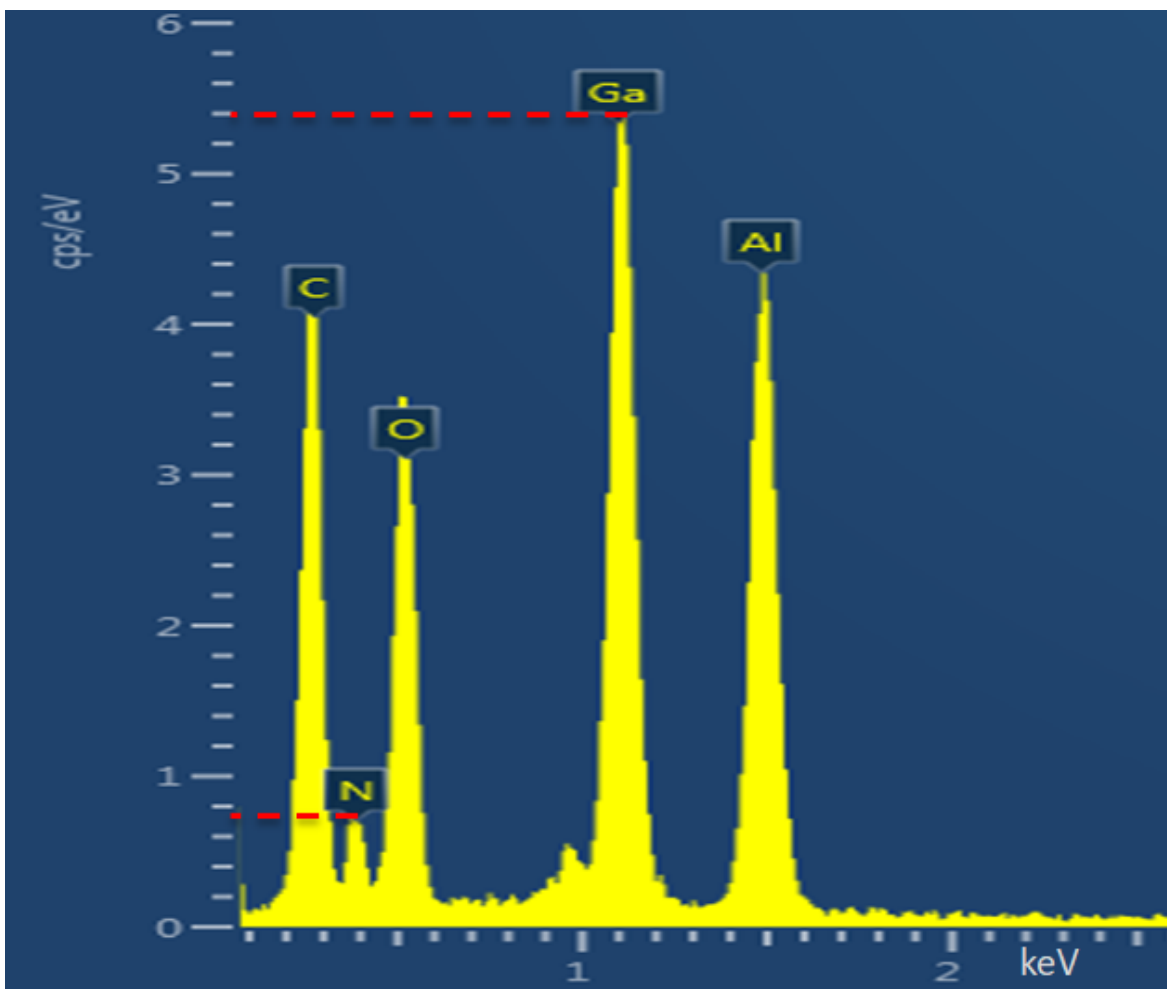


Figure 43: EDX Result for GaN Growth at 225mTorr, 800W

As the GaN layer is relatively thin and the electron beam affects an area of the sample the substrate material is also seen in the resulting EDX measurements. The aluminum and oxygen peaks observed correspond to the sapphire, Al_2O_3 , substrate. The carbon peak corresponds to the required carbon layer applied to the samples required for SEM imaging and EDX measurements. There could also be possible oxygen or carbon contamination resulting for exposure to atmosphere found on the samples contributing to these peaks.

The rough nitrogen to gallium ratios from the EDX measurements shown in Figure 42 and Figure 43 were found to be ≈ 0.174 for the 350mTorr growth and 0.144 for the 225mTorr growth.

Although the peak atomic nitrogen emissions were measured at 225mTorr, the measured nitrogen content for the growth at this pressure was lower than that of the 350mTorr growth. It appears the correlation between plasma conditions and nitrogen incorporation in the deposited material involves more than just the atomic nitrogen content. The plasma density is also lower at 350mTorr than at 225mTorr so the overall amount of nitrogen atoms present also does not appear to solely lead to higher nitrogen content in the resulting growths.

5 Conclusion and Future Work

The DC nitrogen plasma characteristics for the Lakehead University remote plasma-enhanced MOCVD reactor were found to be most strongly affected by changes in chamber pressure. Experimental GaN growths were performed and analyzed at varying chamber pressures and other system parameters kept constant to investigate the resulting effects on growths. It was concluded that the chamber pressure, achievable plasma power, and the resulting plasma conditions are all important parameters to consider when attempts are made to optimize III-N crystal growth conditions.

It was found that as the chamber pressure increased, the plasma temperature and density generally decreased. The effects of varying the chamber pressure was found to have a much greater impact on plasma characteristics at lower pressures, which were from 100 – 300mTorr for these experiments. The effect of varying the applied plasma power was found to have a significantly reduced effect on the plasma when compared to varying the pressure at chamber pressure higher than 100mTorr. From data taken via optical spectroscopy of the ignited plasma, it was found that the atomic nitrogen emissions reach a maximum at a chamber pressure of 225mTorr with an applied plasma power of 800W then decrease for all higher pressures tested.

Results from experimental growths of GaN show the best results, based on XRD measurements measuring crystallinity in the [002] orientation, to occur at chamber pressures from 350 – 450mTorr with 350mTorr providing the best results. The growth performed at 225mTorr, the pressure where the peak atomic nitrogen emissions were found, produced better results than other growths at pressures from 200 – 300mTorr.

Normalized results from the XRD measurements from the experimental GaN growths and normalized plasma parameters found at these settings are shown in Figure 44. Here the trends found as the chamber pressure varies can be seen. As the data point collected at 400mTorr, 800W is assumed to be an outlier as at other applied plasma powers this sharp increase is not seen, the normalized plasma temperature is also shown with the data point at 400mTorr removed.

AFM results and SEM images of the growths performed at the lower pressures, from 200 – 300mTorr show smooth and uniform surfaces. At the higher pressures tested, from 350 – 450mTorr, rough surfaces with elongated particle formations were found. This could be indicative of plasma etching at the lower pressures due to the higher plasma temperatures. There appears to be a required chamber pressure minimum near 350mTorr which produces plasma temperatures low enough to avoid plasma damage of growth surfaces.

SEM images show similar growth rates for all samples. The increased plasma densities and higher atomic nitrogen content at the lower pressures does not appear to directly result in an increased growth rate or higher nitrogen incorporation. EDX measurements show that although the peak atomic nitrogen measurements were found at 225mTorr it did not result in the growth at this pressure having the highest nitrogen content.

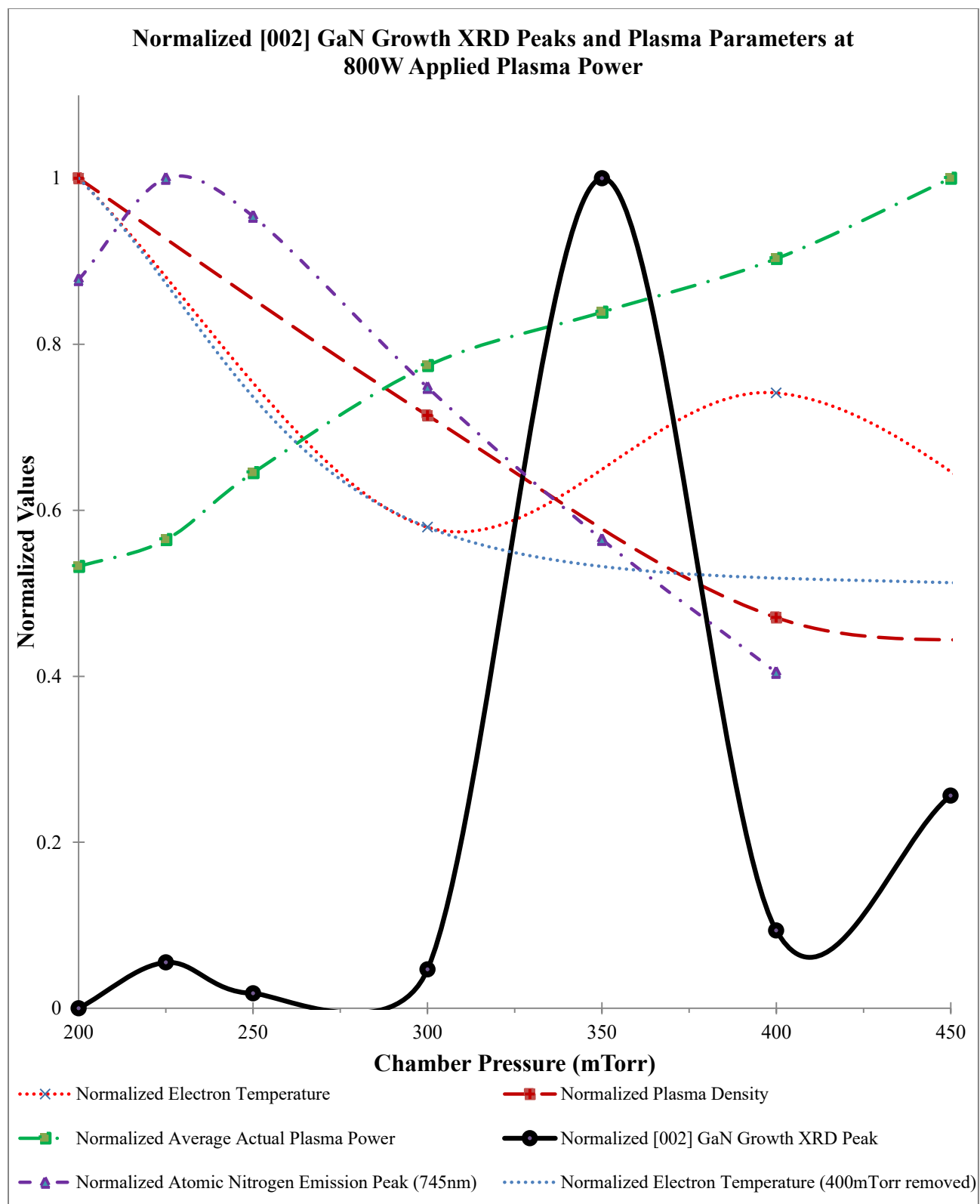


Figure 44: Normalized [002] GaN Growth XRD Peaks and Plasma Parameters at 800W Applied Plasma Power

A combination of all the observed trends shown in Figure 44 and many other unknown factors are likely to be contributing towards the conditions arising at a chamber pressure of 350mTorr and 800W applied plasma power producing an environment favourable for crystalline GaN growth. By comparing these current known trends with future growth results, attempts to better optimize chamber conditions for future III-N growths can be made. These results were presented and published in [20].

Future investigation includes further experimental growths for other III-N materials which are able to be grown in the Lakehead reactor. The other controllable parameters, such as growth temperature or metalorganic and plasma pulse timing could be systematically varied for experimental growths and the resulting effects analyzed in attempts to further optimize growth conditions. Similar investigations while using an RF plasma source could also be conducted and compared to these results using a DC plasma source.

6 References

- [1] *The Blue Laser Diode The Complete Story*. Springer Verlag, 2010.
- [2] H. Yoshida, Y. Yamashita, M. Kuwabara, and H. Kan, “A 342-nm ultraviolet AlGa_N multiple-quantum-well laser diode,” *Nat. Photonics*, vol. 2, no. 9, pp. 551–554, Sep. 2008.
- [3] Z. H. Liu, G. I. Ng, H. Zhou, S. Arulkumaran, and Y. K. T. Maung, “Reduced surface leakage current and trapping effects in AlGa_N/Ga_N high electron mobility transistors on silicon with Si₃N₄/Al₂O₃ passivation,” *Appl. Phys. Lett.*, vol. 98, no. 11, p. 113506, Mar. 2011.
- [4] Department of Physics, Chemistry and Biology, Semiconductor Materials, Linköping University and D. Nilsson, *Doping of high-Al-content AlGa_N grown by MOCVD*. Linköping University Electronic Press, 2014.
- [5] R. J. Goldston and P. H. Rutherford, *Introduction to plasma physics*. Bristol, UK ; Philadelphia: Institute of Physics Pub, 1995.
- [6] F. Chen, *Introduction to Plasma Physics and Controlled Fusion*. Cham: Springer International Publishing, 2016.
- [7] M. Mesrine, N. Grandjean, and J. Massies, “Efficiency of NH₃ as nitrogen source for Ga_N molecular beam epitaxy,” *Appl. Phys. Lett.*, vol. 72, no. 3, pp. 350–352, Jan. 1998.
- [8] S. Strite, “Ga_N, Al_N, and In_N: A review,” *J. Vac. Sci. Technol. B Microelectron. Nanometer Struct.*, vol. 10, no. 4, p. 1237, Jul. 1992.
- [9] D. M. Dobkin and M. K. Zuraw, *Principles of Chemical Vapor Deposition*. Dordrecht: Springer Netherlands, 2003.
- [10] Y. Homma, H. Yamaguchi, and Y. Horikoshi, “Direct comparison of GaAs surface morphology between migration enhanced epitaxy and molecular beam epitaxy using *in situ* scanning electron microscopy,” *Appl. Phys. Lett.*, vol. 68, no. 1, pp. 63–65, Jan. 1996.
- [11] R. P. Vaudo, J. W. Cook, and J. F. Schetzina, “Atomic nitrogen production in nitrogen-plasma sources used for the growth of ZnSe : N and related alloys by molecular-beam epitaxy,” *J. Cryst. Growth*, vol. 138, no. 1–4, pp. 430–436, Apr. 1994.
- [12] W. C. Hughes, “Molecular beam epitaxy growth and properties of Ga_N films on Ga_N/SiC substrates,” *J. Vac. Sci. Technol. B Microelectron. Nanometer Struct.*, vol. 13, no. 4, p. 1571, Jul. 1995.

- [13] R. L. Merlino, "Understanding Langmuir probe current-voltage characteristics," *Am. J. Phys.*, vol. 75, no. 12, pp. 1078–1085, Dec. 2007.
- [14] "Bragg diffraction illustration." [Online]. Available: https://upload.wikimedia.org/wikipedia/commons/c/c0/Bragg_diffraction_2.svg. [Accessed: 08-Mar-2019].
- [15] M. A. Moram and M. E. Vickers, "X-ray diffraction of III-nitrides," *Rep. Prog. Phys.*, vol. 72, no. 3, p. 036502, 2009.
- [16] "Atomic Force Microscopy." [Online]. Available: https://upload.wikimedia.org/wikipedia/commons/7/7c/Atomic_force_microscope_block_diagram.svg. [Accessed: 10-Mar-2019].
- [17] "Schema MEB (en) - Scanning electron microscope - Wikipedia." [Online]. Available: [https://en.wikipedia.org/wiki/Scanning_electron_microscope#/media/File:Schema_MEB_\(en\).svg](https://en.wikipedia.org/wiki/Scanning_electron_microscope#/media/File:Schema_MEB_(en).svg). [Accessed: 11-Mar-2019].
- [18] "Electron Interaction with Matter - Electron microscope - Wikipedia." [Online]. Available: https://en.wikipedia.org/wiki/Electron_microscope#/media/File:Electron_Interaction_with_Matter.svg. [Accessed: 11-Mar-2019].
- [19] "EDX-scheme - Energy-dispersive X-ray spectroscopy - Wikipedia." [Online]. Available: https://en.wikipedia.org/wiki/Energy-dispersive_X-ray_spectroscopy#/media/File:EDX-scheme.svg. [Accessed: 25-Apr-2019].
- [20] B. Kadikoff, R. Dubreuil, J. Tot, and D. Alexandrov, "Investigation into the Characteristics of DC Nitrogen Plasma Used for Group III-N Semiconductor Thin-Film Growths," in *2018 41st International Spring Seminar on Electronics Technology (ISSE)*, Zlatibor, Serbia, 2018, pp. 1–5.